Gondwana Research 25 (2014) 797–819

Contents lists available at ScienceDirect

Gondwana Research

journal homepage: www.elsevier.com/locate/gr

The Paleozoic evolution of Central Tianshan: Geochemical and geochronological evidence

Xuxuan Ma [a], Liangshu Shu [a,*], Joseph G. Meert [b], Jinyi Li [c]

[a] State Key Laboratory for Mineral Deposits Research, Nanjing University, Nanjing 210093, China
[b] University of Florida, Department of Geological Sciences, 241 Williamson Hall, Gainesville, FL 32611, United States
[c] Institute of Geology, Chinese Academy of Geological Sciences, Beijing 100037, China

ARTICLE INFO

Article history:
Received 27 January 2013
Received in revised form 15 April 2013
Accepted 5 May 2013
Available online 10 June 2013

Handling Editor: W.J. Xiao

Keywords:
Granitoids
Zircon
Hf isotopes
Geochemistry
Central Tianshan

ABSTRACT

A suite of Paleozoic granitoids in Central Tianshan was studied for both geochemistry and geochronology in an effort to constrain their origin and tectonic setting. We combined LA-ICP-MS dating of zircon, standard geochemical analyses and Hf-isotopic studies of zircon to develop our tectonic model. Based on our analysis, the granitoids formed in three distinctive stages: ~450–400 Ma, ~370–350 Ma and ca. 340 Ma. The first stage (450–400 Ma) granitoids exhibit metaluminous, magnesian, high-K to shoshonitic characteristics of I-type granitoids (arc-setting), that are enriched in LREE relative to HREE with high $(La/Yb)_{CN}$ values, show negative Eu anomaly and are depleted in Nb, Ta and Ti. This phase of granitoid emplacement was most likely related to the southward subduction of the Paleo-Tianshan Ocean beneath the Tarim block and the subsequent Central Tianshan arc. In contrast, the second stage granitoids (370–350 Ma) are distinctly different and are classified as calc-alkaline or shoshonitic plutons with a weak positive Eu anomaly. Within the second stage granitoids, it appears that the earlier (~365 Ma) granitoids fit within the A-type field whereas the younger (~352 Ma) granitoids plot within the post-collisional potassic field. These granitoids formed during collisions between Central Tianshan and the Tuha terrane that occurred along the northern margin of Central Tianshan. Lastly, the ca. 340 Ma granitoids are typical of volcanic arc granitoids again that probably formed during the northward subduction of the South Tianshan Ocean beneath the Central Tianshan landmass or the subsequent southward subduction of the residual Paleo-Tianshan Ocean.

The Hf isotopic data of zircons from all the studied granitoids were pooled and yielded three prominent Hf T^{C}_{DM} model age populations: ca. 2400 Ma, ca. 1400 Ma and ca. 1100 Ma. The Hf-data shows a significant input of juvenile crust in addition to crustal recycling. We interpret these three phases of juvenile crustal addition to phases of global growth of continental crust (~2400 Ma), the addition of juvenile crust during the breakup of the Columbia supercontinent (~1400 Ma) and the assembly of Rodinia (~1100 Ma).

1. Introduction

The Central Asian Orogenic Belt (CAOB) or the Central Asian Orogenic System (CAOS), also known as "Altaids" in the literature (Sengör et al., 1993) is sandwiched between the European and Siberian Cratons in the north and the Tarim and North China Cratons in the south (Fig. 1a; Xiao et al., 2003; Li, 2006; Charvet et al., 2007; Xiao et al., 2008; Charvet et al., 2011; Han et al., 2011). The arcuate CAOB is one of the largest Phanerozoic orogens on Earth and collectively encompasses immense areas of China, Mongolia, Uzbekistan, Kazakhstan, Russia and their surroundings (Seltmann et al., 2003; Xiao et al., 2003; Levashova et al., 2011). It is also famous for the significant Phanerozoic continental growth and tectonic assembly of continental and oceanic terranes that resulted from the complicated accretion/collision processes of various magmatic arcs, accretionary complexes, microcontinents and seamounts. All these phenomena are thought to be related to the closure of the Paleo-Asian Ocean during the Paleozoic (Coleman, 1989; Zonenshain et al., 1990; Jahn et al., 2000; Shu et al., 2002; Jahn et al., 2004; Xiao et al., 2004; Yakubchuk, 2004; Kröner et al., 2007; Wang et al., 2007a; Windley et al., 2007; Kelty et al., 2008; Xiao et al., 2009; Charvet et al., 2011; Wang et al., 2011a). The CAOB thus provides a perfect laboratory for us to probe the genesis of orogenic belt, the accretion–collision process and the growth of continental crust. While the geography of the CAOB is well established, some crucial questions concerning the architecture's tectonic history remain ambiguous.

The Tianshan orogenic belt (SW CAOB, Fig. 1b), also spelled "Tian Shan" or "Tien Shan" in the literature plays a crucial role in the development of the CAOB (Shu et al., 2004; Kröner et al., 2007; Wang et al., 2007a,b; Windley et al., 2007; Shu et al., 2011a). The Tianshan orogenic belt extends E–W for more than 3000 km from eastern Xinjiang (NW China) to central Uzbekistan and contains the record of multi-phase tectonothermal evolution (Gao et al., 1998; Brookfield, 2000; Shu et al.,

* Corresponding author. Tel.: +86 25 86999386.
E-mail address: lsshu2003@yahoo.com.cn (L. Shu).

1342-937X/$ – see front matter
http://dx.doi.org/10.1016/j.gr.2013.05.015

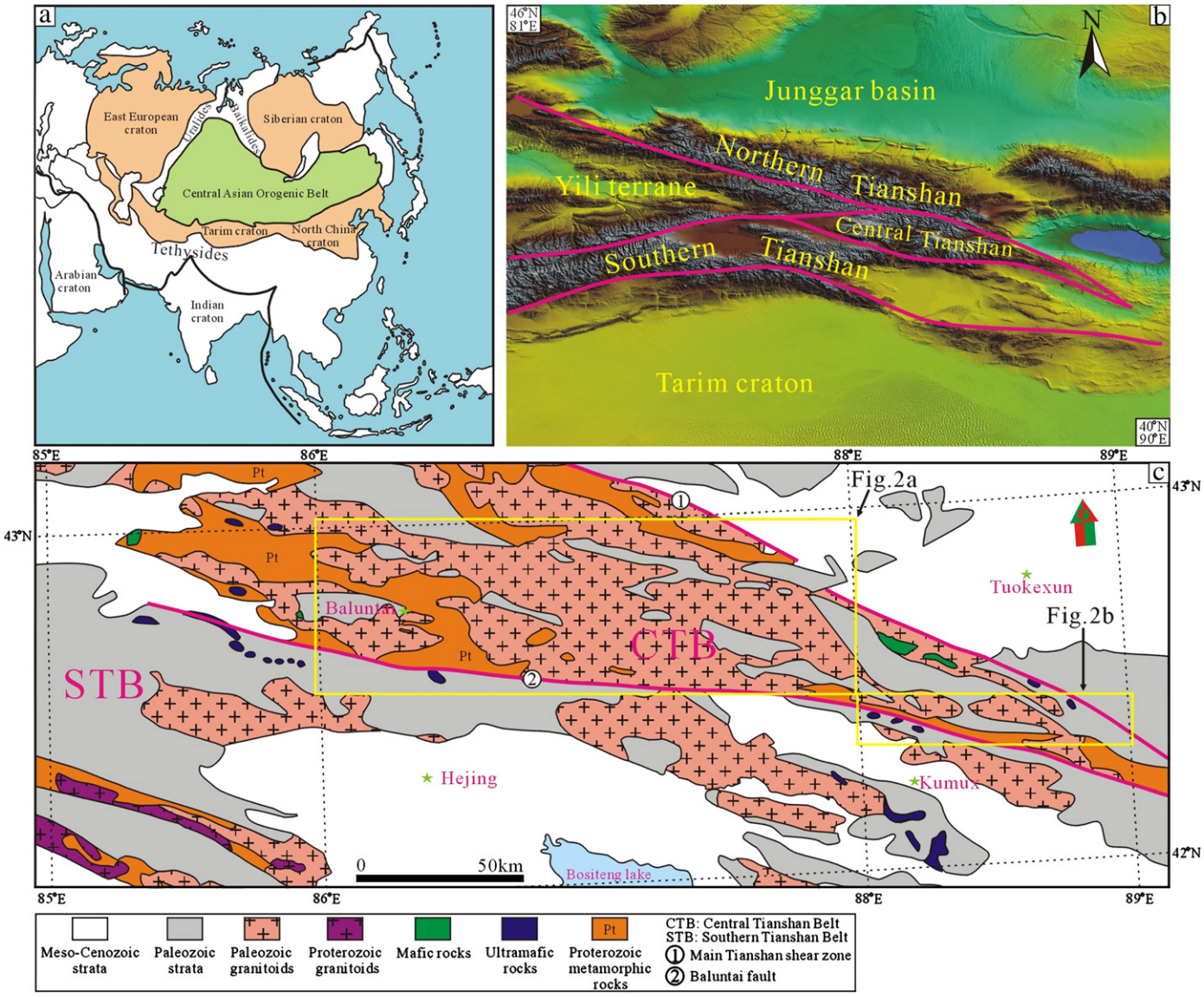

Fig. 1. (a) Tectonic framework of the Central Asian Orogenic Belt (after Xiao et al., 2010). (b) Tectonic framework of Central Tianshan and Tarim. (c) Simplified geological map of Central Tianshan (modified from XBGMR, 1992).

2004; Klemd et al., 2005; Charvet et al., 2007; Xiao et al., 2008; Gao et al., 2009; Xiao et al., 2009; B. Wang et al., 2010). As a late Paleozoic collisional and accretionary orogen, the Tianshan belt was formed by two main stages of N–S directed accretion/collision during Paleozoic (Windley et al., 1990; Allen et al., 1992; Shu et al., 1999; Charvet et al., 2001; Charvet et al., 2004; Wang et al., 2011a), and was strongly modified by subsequent large-scale strike-slip faulting (Laurent–Charvet et al., 2002, 2003).

Tectonically, the Chinese Tianshan (within the Xinjiang area) is subdivided into the South, Central and North Tianshan belts (Shu et al., 1999, 2002; Charvet et al., 2007, 2011). The western segment of the Chinese Tianshan meets the Yili Block (Fig. 1c), that is commonly correlated with the Central Tianshan microcontinent and called the Yili-Central Tianshan terrane (Allen et al., 1992; Gao et al., 1998; Gao and Klemd, 2003). It is also possible that the Yili Block may be regarded as the western equivalent of the North Tianshan volcanic arc. This has been argued on the basis of lithological differences between the Central Tianshan and the Yili Block (see Charvet et al., 2004; Wang et al., 2007b).

The Central Tianshan microcontinent (or Central Tianshan) constitutes a critical component of the Tianshan belt, which in turn is an important part of the CAOB (Charvet et al., 2007; Wang et al., 2008; Lin et al., 2009; B. Wang et al., 2010; Charvet et al., 2011). Therefore a clear understanding of tectonic events within the Central Tianshan will have a direct impact on the evolutionary history of the CAOB.

The paleogeographic evolution of the Paleo-Asian Ocean is controversial due, in no small part, to the fragmentary nature of the blocks within the CAOB. One model posits that during the early Paleozoic, the Paleo-Asian Ocean resembled the current-day situation in the SW Pacific that consists of an archipelago of microcontinents and magmatic arcs (Shu et al., 2001; Windley et al., 2007; Xiao et al., 2008; Han et al., 2010). According to many models, the microcontinents within the CAOB originated from Baltica, Siberia or the Tarim craton (Sengör et al., 1993; Sengör and Natal'in, 1996).

The early Paleozoic development of the CAOB (in general) and the Tarim block and Central Tianshan (in particular) are contentious. This is due to the lack of high-quality paleomagnetic data for the blocks in question (see Collins et al., 2003; Levashova et al., 2011). One model (Wilhem et al., 2012) positions the Tarim block at the northeastern Cimmerian margin of Gondwana with the Central Tianshan components nearby, but scattered across the Paleo-Asian Ocean (de Jong et al., 2006). In contrast, other authors have argued extensively that the Central Tianshan block was part of Tarim during the Precambrian

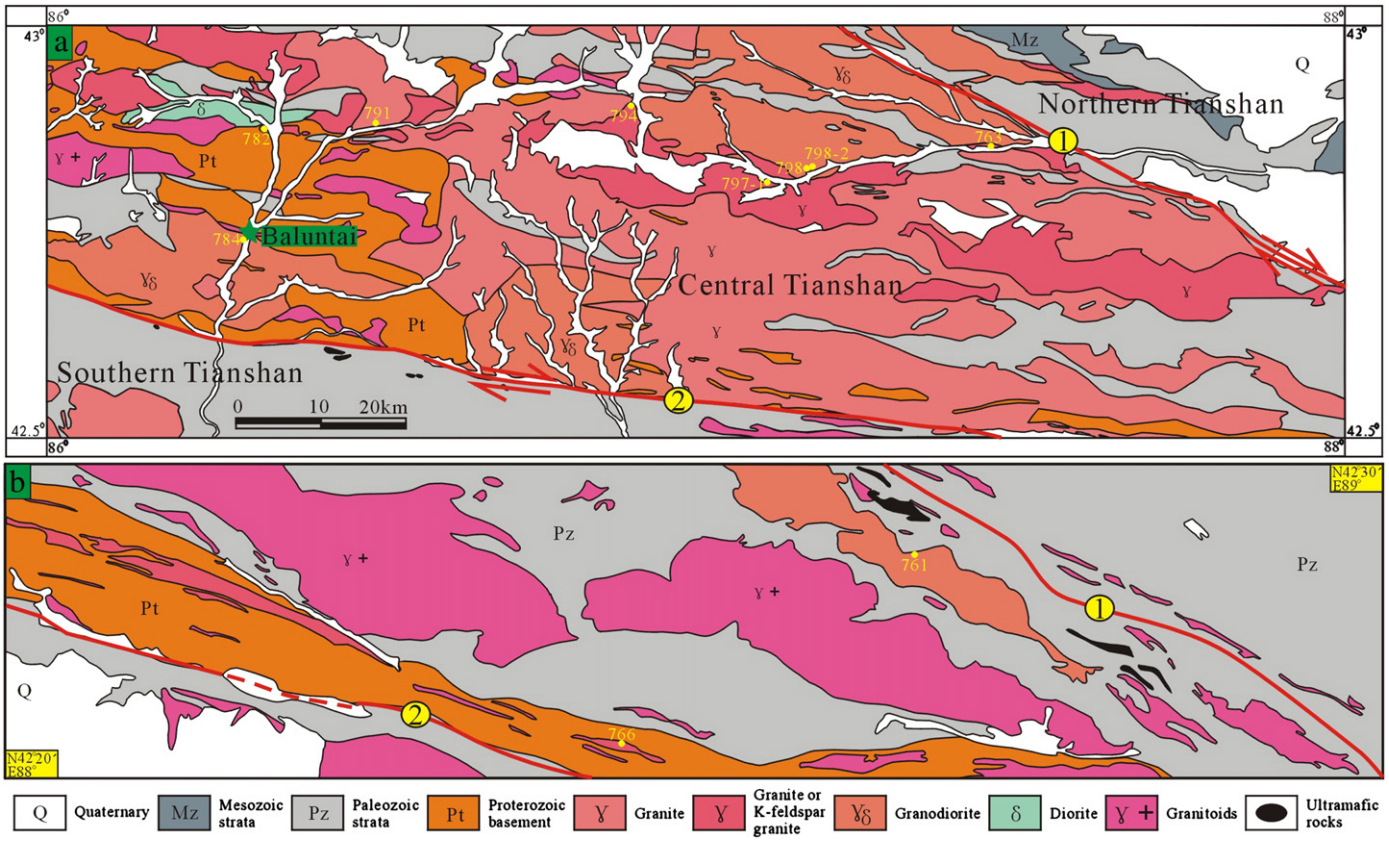

Fig. 2. Detailed geological map of Central Tianshan showing the sampling sites.
Modified from XBGMR (1992).

and became detached during the southward subduction of the Paleo-Asian Ocean beneath Tarim (Li, 1981; Shu et al., 2002; Zhu et al., 2004; Charvet et al., 2007; Wang et al., 2008; Lin et al., 2009; Charvet et al., 2011; Lei et al., 2011; Ma et al., 2012a,b,c). In those models, the "South Tianshan Ocean" was opened as a back-arc basin between Tarim and the separated Central Tianshan block during the Ordovician–Silurian (Ma et al., 1993). The Central Tianshan existed as a microcontinental arc until the Carboniferous (Xiao et al., 2008).

Based on the kinematic analyses of deformation structures, the southward subduction model of the South Tianshan Ocean beneath the Tarim block leading to the closure of the Southern Tianshan back-arc basin was proposed (Shu et al., 2002, 2004; Charvet et al., 2007; Wang et al., 2007a,b; Lin et al., 2009; B. Wang et al., 2010; Charvet et al., 2011; Wang et al., 2011a). Alternatively, analyses of sedimentary, structural and magmatic records, led other workers to propose a scenario whereby the northward subduction of the South Tianshan Ocean beneath the Yili-Central Tianshan terrane triggered the closure of the South Tianshan Ocean (Allen et al., 1992; Gao et al., 1998; Xiao et al., 2004; Yang et al., 2006; Biske and Seltmann, 2010; Dong et al., 2011; He et al., 2012; Xiao et al., 2012). A third approach was proposed by Gao et al. (2009) and Ge et al. (2012) wherein dual-polarity subduction of the South Tianshan Ocean took place. At present, the polarity of subduction remains an open question.

By far the most voluminous and significant feature of the Central Tianshan is the Paleozoic granitoid intrusions. Previous studies indicate that these resulted from multi-stage subduction, collision and post-collision effects (Dong et al., 2011; Ma et al., 2012c). Given the variety of these intrusions, it is possible that detailed studies will provide valuable clues to the evolution history of continental crust in the Central Tianshan. In particular, it is important to carefully establish both the temporal and tectonic frameworks for these granitoid intrusions. In addition, since the development of the CAOB may include the formation of a significant portion of new continental crust, it is important to detail any juvenile contributions in the Central Tianshan granitoids (Sengör et al., 1993; Jahn et al., 2000, 2004; Kovalenko et al., 2004; Windley et al., 2007).

Table 1
Simple petrological description of the studied samples in Central Tianshan.

Sample no.	Field name	Petrological name	Major minerals	GPS
761	Gneissic granite	Granodiorite	Pl: 70–75%, Qtz: 10–15%, Bt: 5–10%	N42°27.11′E88°39.819′
763	K-feldspar granite	K-feldspar granite	Kfs: 50–60%, Qtz: 20–25%, Pl: 10–15%	N42°51.087′E87°27.545′
766	K-feldspar granite	K-feldspar granite	Kfs: 40–50%, Qtz: 20–30%, Pl: 15–20%	N42°20.917′E88°26.912′
782	K-feldspar granite	K-feldspar granite	Kfs: 40–50%, Pl: ~30%, Qtz: ~20%	N42°52.426′E86°20.948′
784	Granodiorite	Granodiorite	Pl: 50–60%, Kfs: 15–20%, Qtz: ~10%, Bt: ~10%	N42°44.588′E86°18.345′
791	K-feldspar granite	K-feldspar granite	Kfs: 40–45%, Pl: 20–30%, Qtz: 20–25%	N42°52.689′E86°30.455′
794	K-feldspar granite	Biotite K-feldspar granite	Kfs: 30–40%, Pl: ~20%, Qtz: ~25%, Bt: ~15%	N42°54.36′E86°54.039′
797-1	K-feldspar granite	Granite	Qtz: 30-40%, Pl: ~40%, Kfs: 10%, Bt: ~10%	N42°48.758′E87°06.758′
798	Granite	Granodiorite	Pl: ~75%, Qtz: ~10%, Bt: ~15%	N42°48.975′E87°10.951′
798-2	Granodiorite	Diorite	Pl: ~65%, Hbl: ~15%, Qtz: ~15%, Bt: ~5%	N42°48.975′E87°10.951′

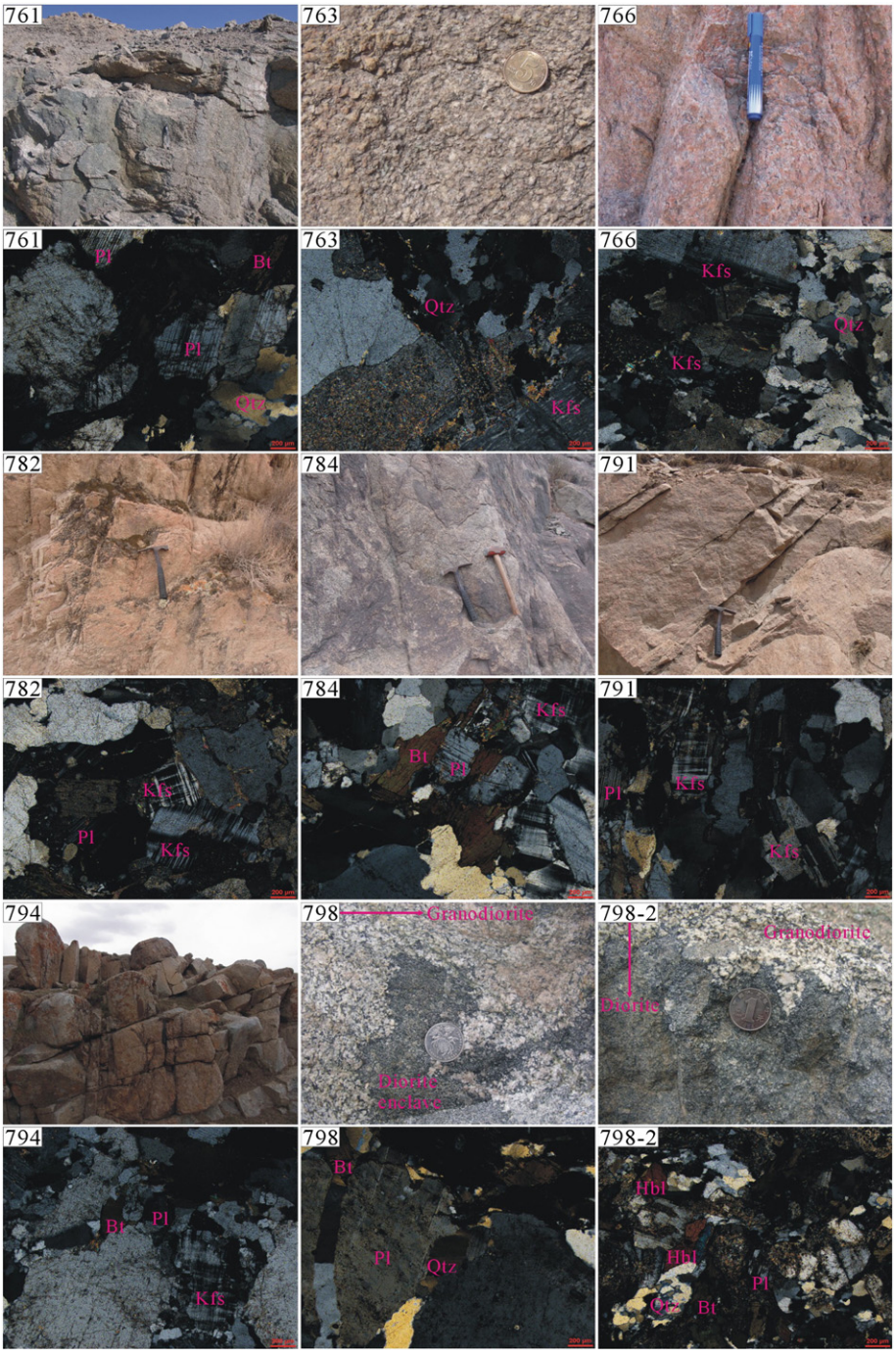

Fig. 3. Field photos and photomicrographs of the granitoids examined in this study. Bt, biotite; Hbl, hornblende; Kfs, K-feldspar; Pl, plagioclase; Qtz, quartz.

In this contribution, we present new zircon U–Pb geochronological data from the Central Tianshan granitoid rocks, Lu–Hf isotopic data as well as major and trace element geochemistry to improve our understanding of the tectonic history of the region during the Paleozoic. These new data will allow us to decipher the tectonic setting of the granitoids, the contributions of mantle components to the crust and the geodynamic setting of Central Tianshan and its role in the overall development of the CAOB.

2. Geological setting

The Chinese Tianshan belt comprises an important tectonic collage within the immense CAOB (Hendrix et al., 1992; Yang et al., 2007). Tectonically, the Chinese Tianshan range can be subdivided into the Northern, Central and Southern Tianshan domains from north to south, which are fringed by two major sutures: the Northern Central Tianshan suture and Southern Central Tianshan suture (Xiao et al., 2009; Dong et al., 2011; Fig. 1b and c). The Northern Tianshan belt comprises Carboniferous clastic sedimentary rocks and andesites (Charvet et al., 2007), and the Southern Tianshan is characterized by late Cambrian to Ordovician sediments with interlayered volcanic rocks (Shu et al., 2002, 2004).

The Central Tianshan domain can be further subdivided into Western and Eastern portions, that have different rock assemblages. The Western part, namely the Yili terrane, is dominated by a thick sequence of Proterozoic–Paleozoic sedimentary rocks (Che et al., 1994; Wang et al.,

Table 2
Early Paleozoic geochronological data from Central Tianshan. Ages of granitoids related to the southward subduction of the Paleo-Tianshan ocean.

No.	Lithology	Location	Age (Ma)	Method	References
1	Granodioritic gneiss	Sangshuyuanzi	481 ± 17	SHRIMP	Li et al. (2009)
2	Granitic Gneiss	Sangshuyuanzi	475.7 ± 1.6	LA-ICPMS	Huang et al. (2012)
3	Granodiorite	Baluntai	475.1 ± 1.7	LA-ICPMS	Ma et al. (2012c)
4	Diorite	Baluntai	473.7 ± 1.6	LA-ICPMS	
5	Gneissic granite	Tianhu	466.5 ± 9.8	SHRIMP	Hu et al. (2007)
6	Diorite	Tuzileike	460 ± 11	Rb-Sr	Gu and Yang (1990)
7	Biotite granite	Baluntai	456.2 ± 0.6	LA-ICPMS	Han et al. (2004)
8	Granite	Baoertu	455.6 ± 1.8	LA-ICPMS	X.J. Wang et al. (2011)
9	Gneissic granite	Kumishi	452 ± 19	Rb-Sr	Ma et al. (1993)
10	Mylonitized granite	Bingdaban	441.6 ± 3.8	SHRIMP	Zhu and Song (2006)
11	Diorite	Hongliuhe	441.4 ± 1.6	LA-ICPMS	Li et al.(2001)
12	Granite	Hongliuhe	440.9 ± 3.1	LA-ICPMS	
13	Augen granite	Gangou	428 ± 10	SHRIMP	Shi et al. (2007)
14	Monzodiorite	Xiaoyanchi	427 ± 8	SHRIMP	Wang et al. (2006)
15	Quartz dioritic gneiss	Xingxingxia	425	LA-ICPMS	He et al. (2012)
16	Granite	Maanqiao	424.5 ± 2.6	LA-ICPMS	Dong et al. (2011)
17	Granodiorite	Xingxingxia	424.9 ± 5.8	LA-ICPMS	Lei et al. (2011)
18	Granite	Kumishi	424.1 ± 1.1	TIMS	Xu et al. (2006)
19	Gneissic granite	Kawabulake	424.2 ± 3.4	LA-ICPMS	Peng et al. (2012)
20	Mylonitized volcanics		422 ± 56	Rb-Sr	Che et al. (1994)

2007b; Dong et al., 2011). Our study centers on the eastern part of the Central Tianshan domain (Central Tianshan for short in the following discussion), that is fringed by the northern Main Tianshan shear zone and the southern Baluntai fault (Charvet et al., 2007; Lin et al., 2009; Charvet et al., 2011; Wang et al., 2011a,b; Ma et al., 2012a,b,c). The study area is located in the Baluntai, Alagou and their surroundings, that are the heartland of Central Tianshan (Fig. 2). The simple petrological description for these rocks is shown in Table 1 and Fig. 3.

Several distinguishable petrotectonic assemblages could be identified in the Central Tianshan from oldest to youngest these are: (a) Proterozoic basement, (b) Ordovician–Early Devonian arc-related volcanic rocks and intrusions and (c) unconformably-overlying Carboniferous and post-Carboniferous sedimentary cover (Shu et al., 2002, 2011a; Wang et al., 2011a). The Precambrian basement mainly cropped out in the Baluntai region (XBGMR, 1993). Ages of the basement rocks are derived from a granitic gneiss dated to 930–940 Ma (Chen et al., 2009), and from an orthogneiss dated to ca. 700 Ma (Yang et al., 2006).

The assemblages of basalts, dacites, andesites, rhyolites, graywackes and flysch are a conspicuous feature of the early Paleozoic Central Tianshan that have undergone a regional greenschist-facies metamorphism (Shu et al., 1998; Charvet et al., 2001; Laurent-Charvet et al., 2002; Shu et al., 2002; Laurent-Charvet et al., 2003; Charvet et al., 2004). Furthermore, voluminous early Paleozoic continental magmatic arc-related granitoids are exposed in the Central Tianshan, that may have formed in a subduction-related setting (Table 2).

Fig. 4. Representative cathodoluminescence pictures of magmatic zircons in granitoids from Central Tianshan. U–Pb age spot with diameter of 25 μm and Lu–Hf spot with diameter of 35 μm are indicated by the small solid circle and big dashed circle, respectively.

Table 3
LA-ICPMS U–Pb age data for zircons from the granitoid rocks in Central Tianshan.

Spots	Corrected ratios						Corrected ages (Ma)									
	$^{207}Pb/^{206}Pb$	1s	$^{207}Pb/^{235}U$	1s	$^{206}Pb/^{238}U$	1s	$^{207}Pb/^{206}Pb$	1s	$^{207}Pb/^{235}U$	1s	$^{206}Pb/^{238}U$	1s	concordance	^{232}Th(ppm)	^{238}U(ppm)	Th/U
761 Granodiorite																
761-01	0.05459	0.00173	0.40845	0.01305	0.05427	0.00094	395	41	348	9	341	6	102	105	111	0.94
761-02	0.053	0.0012	0.40794	0.00965	0.05583	0.00088	329	27	347	7	350	5	99	187	174	1.07
761-03	0.05167	0.00096	0.40431	0.00813	0.05676	0.00083	271	22	345	6	356	5	97	313	260	1.20
761-04	0.05435	0.00183	0.42758	0.01438	0.05706	0.00105	386	43	361	10	358	6	101	205	213	0.96
761-05	0.05526	0.00182	0.42526	0.0139	0.05582	0.00094	423	43	360	10	350	6	103	240	228	1.05
761-06	0.0567	0.00122	0.42658	0.00972	0.05457	0.00087	480	25	361	7	343	5	105	296	536	0.55
761-07	0.05165	0.00153	0.40053	0.01204	0.05625	0.00095	270	39	342	9	353	6	97	78	132	0.59
761-08	0.05078	0.00182	0.39738	0.01414	0.05677	0.00106	231	48	340	10	356	6	96	117	151	0.77
761-09	0.05428	0.0015	0.4266	0.01173	0.057	0.00086	383	35	361	8	357	5	101	240	188	1.28
761-10	0.05348	0.00184	0.41822	0.01426	0.05672	0.00106	349	44	355	10	356	6	100	85	123	0.69
761-11	0.05403	0.00132	0.4167	0.01039	0.05594	0.00085	372	30	354	7	351	5	101	164	211	0.77
761-12	0.05191	0.00396	0.41714	0.03057	0.05827	0.00174	281	113	354	22	365	11	97	221	199	1.11
761-13	0.05372	0.00185	0.41486	0.01401	0.05601	0.00092	359	47	352	10	351	6	100	132	163	0.81
761-14	0.05269	0.00107	0.40306	0.00872	0.05548	0.00085	315	24	344	6	348	5	99	341	318	1.07
761-15	0.05489	0.00198	0.42384	0.01491	0.056	0.00093	408	49	359	11	351	6	102	153	193	0.80
763 K-feldspar granite																
763-01	0.0595	0.00156	0.44739	0.01169	0.05454	0.00081	585	32	375	8	342	5	110	184	234	0.79
763-02	0.05974	0.00142	0.44001	0.01054	0.05343	0.00078	594	28	370	7	336	5	110	390	602	0.65
763-03	0.09127	0.00108	3.12216	0.04546	0.24811	0.00345	1452	12	1438	11	1429	18	102	452	524	0.86
763-04	0.05298	0.00305	0.39982	0.02216	0.05475	0.00125	328	84	342	16	344	8	99	94	386	0.24
763-05	0.04855	0.00155	0.35408	0.01137	0.05291	0.00099	126	42	308	9	332	6	93	759	590	1.29
763-06	0.04715	0.00402	0.35701	0.02892	0.05479	0.00181	57	117	310	22	344	11	90	611	509	1.20
763-07	0.05735	0.00297	0.4233	0.02113	0.05354	0.00112	505	73	358	15	336	7	107	848	529	1.60
763-08	0.05097	0.00082	0.37491	0.00677	0.05336	0.00077	239	19	323	5	335	5	96	476	452	1.05
763-09	0.05558	0.00144	0.41338	0.01065	0.05394	0.00078	436	32	351	8	339	5	104	374	386	0.97
763-10	0.05143	0.00124	0.37586	0.00954	0.05301	0.00089	260	30	324	7	333	5	97	1601	1591	1.01
763-11	0.0605	0.00123	0.43977	0.00926	0.05273	0.00075	622	23	370	7	331	5	112	458	638	0.72
763-12	0.0529	0.00114	0.39324	0.00883	0.05392	0.00079	325	26	337	6	339	5	99	583	782	0.75
763-13	0.06074	0.00361	0.45022	0.02571	0.05382	0.00127	630	82	377	18	338	8	112	57	417	0.14
763-14	0.06287	0.00123	0.4618	0.00948	0.05328	0.00076	704	22	386	7	335	5	115	632	819	0.77
763-15	0.05699	0.00163	0.4277	0.01217	0.05445	0.00086	491	36	362	9	342	5	106	1332	1230	1.08
766 K-feldspar granite																
766-01	0.04891	0.00111	0.4369	0.01032	0.06481	0.00103	144	28	368	7	405	6	91	292	188	1.55
766-02	0.05462	0.00091	0.48235	0.00885	0.06407	0.00092	397	19	400	6	400	6	100	305	275	1.11
766-03	0.0745	0.00104	0.67189	0.01088	0.06543	0.00092	1055	15	522	7	409	6	128	1128	2787	0.40
766-04	0.05709	0.00163	0.48899	0.01394	0.0622	0.0011	495	33	404	10	389	7	104	600	966	0.62
766-05	0.05866	0.00503	0.50612	0.04159	0.06267	0.00194	555	125	416	28	392	12	106	68	36	1.89
766-06	0.05528	0.00131	0.48586	0.01184	0.06377	0.00097	424	29	402	8	399	6	101	132	92	1.43
766-07	0.0545	0.00088	0.47726	0.00849	0.06353	0.00088	392	18	396	6	397	5	100	632	595	1.06
766-08	0.05344	0.00115	0.3398	0.00774	0.0462	0.00076	348	25	297	6	291	5	102	2395	6822	0.35
766-09	0.05666	0.00128	0.51155	0.01178	0.06548	0.00095	478	27	419	8	409	6	102	205	162	1.27
766-10	0.05997	0.00141	0.51929	0.01248	0.06283	0.00094	602	27	425	8	393	6	108	171	108	1.58
766-11	0.05601	0.00276	0.50481	0.02399	0.06537	0.00133	453	69	415	16	408	8	102	201	94	2.12
766-12	0.05477	0.0038	0.47206	0.03192	0.06254	0.00144	403	110	393	22	391	9	101	36	24	1.51
766-13	0.05319	0.00079	0.46527	0.00777	0.06346	0.00088	337	17	388	5	397	5	98	673	642	1.05
766-14	0.05506	0.00105	0.47914	0.00979	0.06317	0.00095	415	22	397	7	395	6	101	295	268	1.10
766-15	0.05621	0.00157	0.49	0.01374	0.06326	0.001	461	35	405	9	395	6	103	170	87	1.96
782 K-feldspar granite																
782-01	0.05434	0.00082	0.52002	0.00895	0.06941	0.00099	385	17	425	6	433	6	98	191	469	0.41
782-02	0.05495	0.0021	0.52823	0.01956	0.06973	0.00118	410	53	431	13	435	7	99	61	148	0.41
782-03	0.0544	0.00484	0.51818	0.0441	0.06917	0.00223	388	133	424	29	431	13	98	220	408	0.54
782-04	0.05844	0.00308	0.56146	0.02859	0.06965	0.00154	546	73	452	19	434	9	104	910	1376	0.66
782-05	0.05457	0.00108	0.51924	0.01104	0.06899	0.00104	395	23	425	7	430	6	99	264	638	0.41
782-06	0.0554	0.00101	0.52833	0.01015	0.06918	0.00095	428	21	431	7	431	6	100	348	452	0.77
782-07	0.05526	0.00083	0.53351	0.00911	0.07003	0.00099	423	17	434	6	436	6	100	443	857	0.52
782-08	0.05491	0.00086	0.52911	0.00926	0.06989	0.00099	409	18	431	6	435	6	99	233	386	0.60
782-09	0.05556	0.00116	0.54005	0.0116	0.07049	0.001	435	24	438	8	439	6	100	407	737	0.55
782-10	0.05425	0.00219	0.51142	0.02045	0.06835	0.00133	381	55	419	14	426	8	98	569	719	0.79
782-11	0.05411	0.00186	0.5171	0.01752	0.06933	0.00119	376	46	423	12	432	7	98	349	583	0.60
782-12	0.05486	0.0012	0.53079	0.01192	0.07018	0.00101	407	26	432	8	437	6	99	252	406	0.62
782-13	0.05588	0.00085	0.53766	0.00931	0.06978	0.00099	448	17	437	6	435	6	100	389	616	0.63
782-14	0.0559	0.0015	0.53611	0.0149	0.06957	0.00116	448	33	436	10	434	7	100	362	507	0.71
784 Granodiorite																
784-01	0.05564	0.00154	0.55387	0.01561	0.0722	0.00119	438	35	448	10	449	7	100	163	230	0.71
784-02	0.05519	0.00099	0.54197	0.01068	0.07124	0.00108	420	20	440	7	444	6	99	211	240	0.88
784-03	0.05464	0.00089	0.53749	0.00983	0.07135	0.00106	398	19	437	6	444	6	98	309	405	0.76
784-04	0.05639	0.00147	0.55496	0.01486	0.07135	0.00118	468	32	448	10	444	7	101	153	186	0.82
784-05	0.05587	0.00083	0.55225	0.0092	0.07169	0.00099	447	17	446	6	446	6	100	193	284	0.68

Table 3 (*continued*)

Spots	Corrected ratios						Corrected ages (Ma)									
	$^{207}Pb/^{206}Pb$	1s	$^{207}Pb/^{235}U$	1s	$^{206}Pb/^{238}U$	1s	$^{207}Pb/^{206}Pb$	1s	$^{207}Pb/^{235}U$	1s	$^{206}Pb/^{238}U$	1s	concordance	^{232}Th(ppm)	^{238}U(ppm)	Th/U
784 Granodiorite																
784-06	0.05677	0.0012	0.57719	0.01296	0.07374	0.00115	483	24	463	8	459	7	101	173	203	0.85
784-07	0.05648	0.00097	0.56378	0.01056	0.07241	0.00103	471	19	454	7	451	6	101	114	183	0.62
784-08	0.05667	0.00129	0.56922	0.01324	0.07286	0.00106	479	27	458	9	453	6	101	67	117	0.57
784-09	0.05569	0.00099	0.56983	0.01095	0.07422	0.00107	440	20	458	7	462	6	99	136	170	0.80
784-10	0.05717	0.00166	0.58133	0.01673	0.07374	0.00113	498	37	465	11	459	7	101	173	234	0.74
784-11	0.05642	0.00115	0.55654	0.0117	0.07155	0.00099	469	24	449	8	445	6	101	209	290	0.72
784-12	0.05857	0.00172	0.58002	0.01684	0.07183	0.00113	551	37	464	11	447	7	104	118	199	0.59
784-13	0.05769	0.00127	0.58029	0.0134	0.07295	0.00115	518	25	465	9	454	7	102	110	234	0.47
784-14	0.05607	0.00213	0.55919	0.0206	0.07235	0.0013	455	50	451	13	450	8	100	193	369	0.52
784-15	0.05671	0.00153	0.57811	0.0158	0.07392	0.0012	480	33	463	10	460	7	101	115	189	0.61
791 K-feldspar granite																
791-01	0.05105	0.00132	0.41282	0.01084	0.05887	0.00091	243	33	351	8	369	6	95	159	205	0.78
791-02	0.05424	0.00149	0.53441	0.015	0.07149	0.00124	381	34	435	10	445	7	98	295	944	0.31
791-03	0.05377	0.00167	0.42596	0.01301	0.05746	0.00089	361	41	360	9	360	5	100	68	132	0.52
791-04	0.05499	0.001	0.44415	0.00854	0.05858	0.0008	412	21	373	6	367	5	102	105	418	0.25
791-05	0.05465	0.00165	0.44151	0.01308	0.0586	0.00089	398	40	371	9	367	5	101	279	317	0.88
791-06	0.05316	0.00102	0.42981	0.00865	0.05865	0.00082	336	22	363	6	367	5	99	93	267	0.35
791-07	0.05394	0.00135	0.43225	0.01089	0.05813	0.00085	369	31	365	8	364	5	100	86	404	0.21
791-08	0.05592	0.00113	0.44905	0.00944	0.05825	0.00082	449	24	377	7	365	5	103	193	246	0.79
791-09	0.05393	0.00138	0.43588	0.01118	0.05862	0.00086	368	32	367	8	367	5	100	345	354	0.97
794 Biotite K-feldspar granite																
794-01	0.05354	0.00147	0.39387	0.01099	0.05335	0.00081	352	36	337	8	335	5	101	145	91	1.60
794-02	0.05392	0.00087	0.40043	0.00719	0.05386	0.00076	368	19	342	5	338	5	101	820	523	1.57
794-03	0.05597	0.00216	0.41374	0.01563	0.05361	0.00094	451	53	352	11	337	6	104	193	190	1.01
794-04	0.05344	0.00162	0.40161	0.01229	0.05449	0.00091	348	40	343	9	342	6	100	71	124	0.57
794-05	0.05468	0.0013	0.39726	0.00972	0.05268	0.00079	399	29	340	7	331	5	103	149	163	0.92
794-06	0.06392	0.00157	0.4602	0.0117	0.05222	0.00085	739	28	384	8	328	5	117	790	476	1.66
794-07	0.05593	0.00124	0.41169	0.00956	0.05338	0.00081	450	26	350	7	335	5	104	265	290	0.91
794-08	0.05161	0.00124	0.38832	0.00965	0.05456	0.00084	268	30	333	7	342	5	97	221	288	0.77
794-09	0.05511	0.00126	0.40571	0.00947	0.0534	0.00077	417	28	346	7	335	5	103	502	426	1.18
794-10	0.05358	0.00159	0.40832	0.01209	0.05528	0.00088	353	39	348	9	347	5	100	288	351	0.82
794-11	0.05293	0.00099	0.40043	0.00796	0.05488	0.00077	326	22	342	6	344	5	99	789	511	1.55
794-12	0.0534	0.00099	0.39573	0.00785	0.05375	0.00077	346	22	339	6	338	5	100	715	505	1.42
794-13	0.05809	0.00316	0.44044	0.02298	0.05505	0.0012	533	76	371	16	345	7	108	324	268	1.21
794-14	0.05409	0.00163	0.41408	0.01255	0.05551	0.00092	375	39	352	9	348	6	101	238	149	1.60
794-15	0.05082	0.00126	0.38731	0.00993	0.05529	0.00093	233	30	332	7	347	6	96	201	281	0.72
797-1 Granite																
797-1-01	0.0545	0.00117	0.41873	0.00926	0.05573	0.00079	392	26	355	7	350	5	101	434	303	1.43
797-1-02	0.0556	0.0012	0.41585	0.00936	0.05426	0.00079	436	26	353	7	341	5	104	448	349	1.28
797-1-03	0.05504	0.00112	0.41185	0.00856	0.05428	0.00074	414	24	350	6	341	5	103	288	463	0.62
797-1-04	0.05666	0.00116	0.42178	0.00884	0.05399	0.00074	478	24	357	6	339	5	105	467	387	1.21
797-1-05	0.05376	0.00096	0.41246	0.00806	0.05566	0.00083	361	21	351	6	349	5	101	756	409	1.85
797-1-06	0.05377	0.0022	0.41451	0.01647	0.05593	0.001	361	57	352	12	351	6	100	306	227	1.35
797-1-07	0.05486	0.00082	0.41427	0.00687	0.05478	0.00074	407	17	352	5	344	5	102	752	618	1.22
797-1-08	0.05497	0.00091	0.41137	0.00742	0.05428	0.00075	411	19	350	5	341	5	103	469	346	1.36
797-1-09	0.05577	0.00672	0.41877	0.04738	0.05432	0.00249	443	171	355	34	341	15	104	73	67	1.09
797-1-10	0.05611	0.00164	0.4284	0.01243	0.05538	0.00086	457	37	362	9	347	5	104	412	277	1.49
797-1-11	0.05255	0.00143	0.40766	0.01124	0.05627	0.00085	309	36	347	8	353	5	98	165	101	1.63
797-1-12	0.0578	0.00187	0.43635	0.014	0.05474	0.001	522	39	368	10	344	6	107	987	742	1.33
797-1-13	0.05441	0.00099	0.412	0.00792	0.05492	0.00076	388	21	350	6	345	5	101	1163	553	2.10
797-1-14	0.05511	0.00111	0.43168	0.00919	0.05682	0.00088	417	23	364	7	356	5	102	768	414	1.86
797-1-15	0.05826	0.00135	0.436	0.01028	0.05428	0.00078	540	28	367	7	341	5	108	936	505	1.85
798 Granodiorite																
798-01	0.05385	0.00294	0.40473	0.02155	0.05448	0.00118	365	81	345	16	342	7	101	76	92	0.82
798-02	0.05085	0.00117	0.39175	0.00936	0.05586	0.00082	234	29	336	7	350	5	96	195	140	1.39
798-03	0.05699	0.00217	0.4389	0.01642	0.05585	0.001	491	51	369	12	350	6	105	63	85	0.74
798-04	0.05072	0.00171	0.40602	0.01368	0.05804	0.00097	228	47	346	10	364	6	95	124	122	1.02
798-05	0.0558	0.00107	0.43584	0.00898	0.05664	0.00084	444	22	367	6	355	5	103	490	442	1.11
798-06	0.05678	0.00595	0.432	0.0433	0.05522	0.00193	483	160	365	31	346	12	105	229	201	1.14
798-07	0.05333	0.00179	0.40774	0.01358	0.05549	0.00103	343	43	347	10	348	6	100	247	190	1.30
798-08	0.05574	0.00166	0.41852	0.01239	0.05447	0.00087	442	38	355	9	342	5	104	1180	869	1.36
798-09	0.05212	0.00083	0.4095	0.00721	0.05698	0.00079	291	19	349	5	357	5	98	529	620	0.85
798-10	0.05316	0.00175	0.41687	0.01352	0.05688	0.00093	336	44	354	10	357	6	99	194	210	0.92
798-11	0.0513	0.00118	0.39649	0.00953	0.05604	0.00087	254	29	339	7	351	5	97	254	257	0.99
798-12	0.05386	0.00124	0.41788	0.0097	0.05628	0.0008	365	28	355	7	353	5	101	648	552	1.17
798-13	0.05073	0.00087	0.3972	0.0074	0.0568	0.00082	229	20	340	5	356	5	96	283	389	0.73
798-14	0.05592	0.0016	0.42725	0.01215	0.05542	0.00086	449	36	361	9	348	5	104	379	224	1.69
798-15	0.04696	0.002	0.37188	0.01556	0.05752	0.00115	47	56	321	12	361	7	89	216	164	1.31

(*continued on next page*)

Table 3 (*continued*)

Spots	Corrected ratios						Corrected ages (Ma)									
	$^{207}Pb/^{206}Pb$	1s	$^{207}Pb/^{235}U$	1s	$^{206}Pb/^{238}U$	1s	$^{207}Pb/^{206}Pb$	1s	$^{207}Pb/^{235}U$	1s	$^{206}Pb/^{238}U$	1s	concordance	^{232}Th(ppm)	^{238}U(ppm)	Th/U
798-2 Diorite																
798-2-01	0.05681	0.00097	0.45696	0.00846	0.05835	0.00083	484	19	382	6	366	5	104	1911	1275	1.50
798-2-02	0.0545	0.00075	0.44152	0.00712	0.05876	0.00082	392	16	371	5	368	5	101	2677	1259	2.13
798-2-03	0.05381	0.00091	0.43573	0.0082	0.05874	0.00085	363	20	367	6	368	5	100	810	601	1.35
798-2-04	0.05638	0.00108	0.46372	0.00954	0.05966	0.00088	467	22	387	7	374	5	103	390	308	1.26
798-2-05	0.05477	0.00085	0.46177	0.00823	0.06117	0.0009	403	18	385	6	383	5	101	1747	1033	1.69
798-2-06	0.05617	0.00121	0.456	0.01051	0.05891	0.00095	459	25	381	7	369	6	103	1880	1160	1.62
798-2-07	0.05981	0.00109	0.48037	0.00924	0.05826	0.0008	597	20	398	6	365	5	109	13,328	2524	5.28
798-2-08	0.05734	0.00286	0.4533	0.02193	0.05735	0.0012	505	70	380	15	359	7	106	249	163	1.53
798-2-09	0.05372	0.00128	0.44546	0.01115	0.06018	0.001	359	29	374	8	377	6	99	1503	795	1.89
798-2-10	0.05533	0.00107	0.45847	0.00971	0.06012	0.00094	426	22	383	7	376	6	102	1070	808	1.32
798-2-11	0.05395	0.00122	0.44045	0.0106	0.05922	0.00098	369	27	371	7	371	6	100	7480	2206	3.39
798-2-12	0.05434	0.0013	0.44414	0.01119	0.05929	0.00096	385	29	373	8	371	6	101	581	473	1.23

Although there is still some debate regarding the Tarim origin for the units in the Central Tianshan (Chen et al., 1999; Hu et al., 2000; Xu et al., 2003; He et al., 2012), a number of recent workers view the Central Tianshan as a fragment of the Tarim block that drifted away during the early Paleozoic (Li, 1981; Gao et al., 1998; Shu et al., 1998; Zhu et al., 2004; Charvet et al., 2007; Wang et al., 2008; Gao et al., 2009; Lin et al., 2009; Wang et al., 2011a; Charvet et al., 2011; Shu et al., 2011b; Rojas-Agramonte et al., 2011; Ma et al., 2012a,b,c; Lei et al., 2011; Wilhem et al., 2012).

3. Methods

3.1. U–Pb ages of zircons

Fresh samples were chosen for zircon U–Pb dating. Zircon grains were separated by using the conventional procedures including heavy liquids, magnetic separation and hand-picking under a binocular microscope. Zircon grains were mounted in epoxy resin, and then polished. Cathodoluminescence (CL) pictures (Fig. 4) of the zircons were obtained

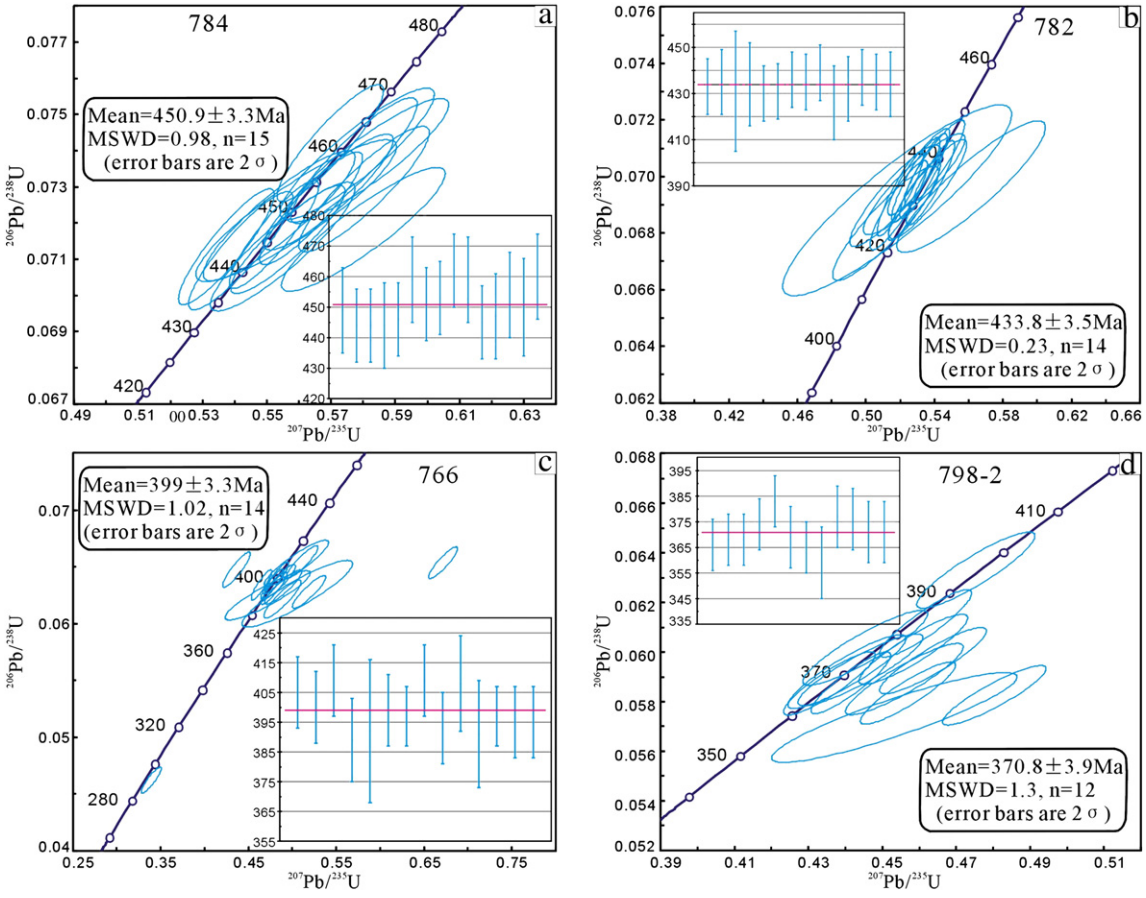

Fig. 5. Four U–Pb concordia diagrams of zircons for the granitoid rocks in Central Tianshan.

using an electron microscope (Quanta 400 FEG) with a Mono CL3 + (Gatan, USA) at the State Key Laboratory of Continental Dynamics at Northwest University, Xi'an.

Zircon U–Pb isotopic analyses were performed at the State Key Laboratory for Mineral Deposits Research, Nanjing University, using an Agilent 7500a ICP-MS attached to a New Wave 213 nm laser ablation system with an in-house sample cell. All analyses were carried out using a beam spot size of ca. 25 μm and a laser frequency of 5 Hz and 60% energy. Detailed analytical procedures and data acquisition are similar to those of Griffin et al. (2004), Wang et al. (2010b) and Ma et al. (2012c).

3.2. Lu–Hf isotope of zircons

Zircon Hf isotope analyses were carried out *in-situ* using a NewWave UP213 laser-ablation microprobe, attached to a Neptune multi-collector ICP-MS at MLR Key Laboratory of Metallogeny and Mineral Assessment, Institute of Mineral Resources, Chinese Academy of Geological Sciences, Beijing. Instrumental conditions and data acquisition were summarized by Wu et al. (2006) and Hou et al. (2007). A stationary spot was used for the present analyses, with a beam diameter of 35 μm. Helium was used as carrier gas to transport the ablated sample from the laser-ablation cell to the ICP-MS torch *via* a mixing chamber mixed with Argon. In order to correct the isobaric interferences of ^{176}Lu and ^{176}Yb on ^{176}Hf, $^{176}Lu/^{175}Lu = 0.02658$ and $^{176}Yb/^{173}Yb = 0.796218$ ratios were determined (Chu et al., 2002). For instrumental mass bias correction Yb isotope ratios were normalized to $^{172}Yb/^{173}Yb$ of 1.35274 (Chu et al., 2002) and Hf isotope ratios to $^{179}Hf/^{177}Hf$ of 0.7325 using an exponential law. The mass bias behavior of Lu was assumed to follow that of Yb, and mass bias correction protocol details were described by Wu et al. (2006) and Hou et al. (2007). Zircon GJ1 was used as the reference standards

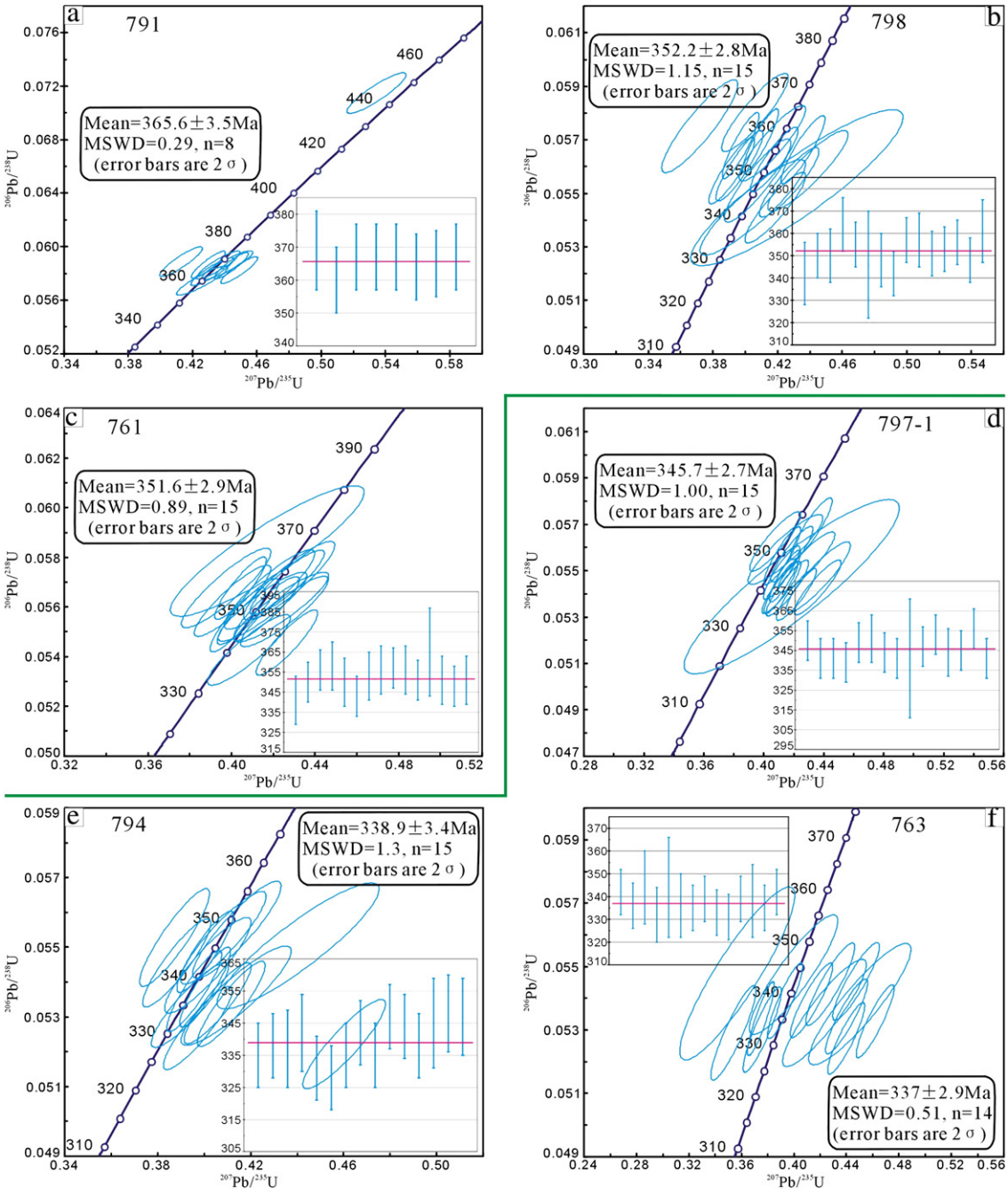

Fig. 6. Six U–Pb concordia diagrams of zircons from the granitoid samples in Central Tianshan.

Table 4
Hf isotopes for zircons from the granitoid rocks in Central Tianshan.

Sample no.	t (Ma)	$^{176}Yb/^{177}Hf$	$^{176}Lu/^{177}Hf$	2σ	$^{176}Hf/^{177}Hf$	2σ	λ	$\varepsilon_{Hf}(t)$	2σ	$f_{Lu/Hf}$	T_{DM1}	2σ	T_{DM}^{C}	2σ
761-01	341	0.010939331	0.000497483	3.91542E−06	0.282533895	1.38444E−05	1.867E−11	−1.40	0.49	−0.985	1003	19	1415	31
761-02	350	0.018601953	0.000835754	2.94094E−05	0.282512459	1.78444E−05	1.867E−11	−2.04	0.63	−0.975	1041	25	1463	40
761-03	356	0.013231933	0.000603374	9.75256E−06	0.282541463	1.38998E−05	1.867E−11	−0.83	0.49	−0.982	995	19	1391	31
761-04	358	0.028245248	0.001265409	4.2478E−06	0.28259673	1.35452E−05	1.867E−11	1.01	0.48	−0.962	934	19	1275	30
761-05	350	0.032531265	0.001315383	1.85975E−05	0.282561448	1.56734E−05	1.867E−11	−0.42	0.55	−0.960	985	22	1360	35
761-06	343	0.014101416	0.000581861	6.43892E−06	0.282528888	1.19172E−05	1.867E−11	−1.56	0.42	−0.982	1012	17	1426	27
761-07	353	0.018868342	0.000832291	4.04851E−05	0.28256261	1.45925E−05	1.867E−11	−0.20	0.52	−0.975	971	20	1349	33
761-08	356	0.028168659	0.001223381	5.18714E−05	0.282593818	1.42111E−05	1.867E−11	0.88	0.50	−0.963	937	20	1282	32
761-09	357	0.018210542	0.000814598	1.44543E−05	0.282551936	1.28953E−05	1.867E−11	−0.49	0.46	−0.975	986	18	1370	29
761-10	356	0.03242996	0.001370265	4.45115E−05	0.28255609	1.40339E−05	1.867E−11	−0.49	0.50	−0.959	994	20	1369	31
761-11	351	0.030198104	0.001286509	5.71156E−05	0.28256337	1.32272E−05	1.867E−11	−0.32	0.47	−0.961	982	19	1355	30
761-12	365	0.023590674	0.000972063	4.45753E−05	0.282539643	1.41792E−05	1.867E−11	−0.79	0.50	−0.971	1007	20	1395	32
761-13	351	0.018871179	0.00083933	9.40566E−06	0.282324515	2.75574E−05	1.867E−11	−8.67	0.98	−0.975	1304	38	1882	61
761-14	348	0.021354295	0.000934563	5.29419E−05	0.282562522	1.45625E−05	1.867E−11	−0.34	0.52	−0.972	974	20	1353	33
761-15	351	0.03478281	0.001382318	9.33603E−05	0.282622619	1.52892E−05	1.867E−11	1.75	0.54	−0.958	900	22	1223	34
763-01	342	0.052162217	0.002039061	3.71053E−05	0.282692564	1.50896E−05	1.867E−11	3.88	0.53	−0.939	815	22	1080	34
763-02	336	0.023237758	0.000902555	4.57349E−06	0.282648655	1.27347E−05	1.867E−11	2.46	0.45	−0.973	852	18	1166	29
763-03	1452	0.019602245	0.000800125	2.13383E−05	0.282704079	1.49068E−05	1.867E−11	29.11	0.53	−0.976	772	21	325	34
763-04	344	0.057659642	0.002276811	2.41558E−05	0.282702982	1.28946E−05	1.867E−11	4.24	0.46	−0.931	805	19	1059	29
763-05	332	0.030479937	0.001226014	2.32536E−05	0.282667644	1.24845E−05	1.867E−11	2.97	0.44	−0.963	833	18	1130	28
763-06	344	0.021076246	0.000805166	4.57198E−05	0.282671522	1.21198E−05	1.867E−11	3.46	0.43	−0.976	818	17	1108	27
763-07	336	0.027731842	0.001133797	9.00267E−06	0.282697044	1.26819E−05	1.867E−11	4.12	0.45	−0.966	789	18	1060	28
763-08	335	0.05553291	0.00213242	1.56119E−05	0.282751834	1.66412E−05	1.867E−11	5.81	0.59	−0.936	731	24	951	37
763-09	339	0.017901668	0.000749923	1.45644E−05	0.282679578	1.26828E−05	1.867E−11	3.65	0.45	−0.977	805	18	1092	28
763-10	333	0.106354625	0.003923224	7.5946E−05	0.282766602	1.45938E−05	1.867E−11	5.90	0.52	−0.882	746	22	944	33
763-11	331	0.03598403	0.001411787	1.57195E−05	0.282718565	1.48231E−05	1.867E−11	4.71	0.52	−0.957	764	21	1018	33
763-12	339	0.030853299	0.001208665	1.78318E−05	0.282690767	1.34568E−05	1.867E−11	3.94	0.48	−0.964	799	19	1074	30
763-13	338	0.021929241	0.0008855	2.5379E−05	0.282687369	1.08174E−05	1.867E−11	3.87	0.38	−0.973	797	15	1077	24
763-14	335	0.03595962	0.001457865	3.03605E−05	0.282682537	1.17786E−05	1.867E−11	3.51	0.42	−0.956	817	17	1098	26
763-15	342	0.019557989	0.000800797	1.44128E−05	0.282685941	1.03783E−05	1.867E−11	3.93	0.37	−0.976	798	15	1077	23
766-01	405	0.098004701	0.003525633	4.16923E−05	0.282507714	1.332E−05	1.867E−11	−1.74	0.47	−0.894	1128	20	1487	30
766-02	400	0.027656356	0.00105887	2.47471E−05	0.282498712	1.74685E−05	1.867E−11	−1.50	0.62	−0.968	1067	25	1468	39
766-03	409	0.032646676	0.001302854	2.11361E−05	0.282501368	1.80123E−05	1.867E−11	−1.28	0.64	−0.961	1070	25	1461	40
766-04	389	0.034129076	0.001277852	1.19252E−05	0.282496231	1.34847E−05	1.867E−11	−1.88	0.48	−0.962	1077	19	1484	30
766-05	392	0.047301784	0.001823116	1.21618E−05	0.282478217	1.69963E−05	1.867E−11	−2.60	0.60	−0.945	1118	24	1531	38
766-06	399	0.026345061	0.001075702	1.08291E−05	0.282470428	1.81447E−05	1.867E−11	−2.53	0.64	−0.968	1107	26	1533	40
766-07	397	0.088436146	0.003354319	1.76541E−05	0.282486401	1.52552E−05	1.867E−11	−2.60	0.54	−0.899	1155	23	1536	34
766-08	291	0.032643248	0.001236938	1.18001E−05	0.282504381	1.39932E−05	1.867E−11	−3.69	0.50	−0.963	1064	20	1520	31
766-09	409	0.034068409	0.001226201	1.0324E−05	0.282526438	2.444E−05	1.867E−11	−0.37	0.87	−0.963	1033	35	1404	55
766-10	393	0.080780794	0.002954789	9.63033E−06	0.282514203	1.63871E−05	1.867E−11	−1.60	0.58	−0.911	1100	24	1469	37
766-11	408	0.027456042	0.001143079	3.1858E−05	0.282525424	1.53525E−05	1.867E−11	−0.40	0.54	−0.966	1032	22	1405	34
766-12	391	0.008946007	0.000382149	5.63478E−06	0.282524397	1.70439E−05	1.867E−11	−0.61	0.60	−0.988	1013	24	1405	38
766-13	397	0.017769394	0.0007177	1.59442E−06	0.282502643	1.3175E−05	1.867E−11	−1.34	0.47	−0.978	1052	18	1455	29
766-14	395	0.038995753	0.001580064	3.45854E−05	0.282541195	1.49845E−05	1.867E−11	−0.24	0.53	−0.952	1021	21	1384	33
766-15	395	0.016775573	0.000701629	2.26679E−05	0.282563072	1.49529E−05	1.867E−11	0.76	0.53	−0.979	967	21	1321	33
782-01	433	0.063233377	0.002445148	2.40663E−05	0.282641204	2.43178E−05	1.867E−11	3.86	0.86	−0.926	899	36	1154	54
782-02	435	0.051842374	0.002035055	5.21843E−05	0.282689306	1.75348E−05	1.867E−11	5.72	0.62	−0.939	820	25	1036	39
782-03	431	0.061389073	0.002406128	3.11045E−05	0.282625237	1.56858E−05	1.867E−11	3.27	0.56	−0.928	922	23	1190	35
782-04	434	0.055070402	0.002120369	6.17182E−05	0.282667753	1.58221E−05	1.867E−11	4.92	0.56	−0.936	853	23	1087	36
782-05	430	0.06778147	0.002586215	4.54759E−05	0.282627844	2.90997E−05	1.867E−11	3.29	1.03	−0.922	922	43	1188	65
782-06	431	0.047987984	0.00184434	4.22783E−05	0.282696338	1.79132E−05	1.867E−11	5.94	0.63	−0.944	805	26	1019	40
782-07	436	0.036660093	0.001440911	3.31473E−05	0.282645904	1.95217E−05	1.867E−11	4.38	0.69	−0.957	868	28	1123	44
782-08	435	0.069296529	0.002656401	4.85234E−05	0.282623507	2.21987E−05	1.867E−11	3.22	0.79	−0.920	931	33	1196	50
782-09	439	0.053932562	0.002146559	7.49036E−05	0.282598847	2.2914E−05	1.867E−11	2.57	0.81	−0.935	953	33	1241	51
782-10	426	0.062818597	0.00243519	2.69884E−05	0.282689954	1.93886E−05	1.867E−11	5.44	0.69	−0.927	828	28	1047	44
782-11	432	0.069530187	0.002689562	7.45159E−05	0.28265382	1.7221E−05	1.867E−11	4.22	0.61	−0.919	887	25	1130	39
782-12	437	0.065196694	0.002518666	3.90908E−05	0.282709808	2.68819E−05	1.867E−11	6.35	0.95	−0.924	800	40	998	60
782-13	435	0.067200798	0.002593282	5.44493E−05	0.282703766	2.49313E−05	1.867E−11	6.07	0.88	−0.922	811	37	1014	56
782-14	434	0.064224096	0.00253109	1.98077E−05	0.282650114	2.8748E−05	1.867E−11	4.17	1.02	−0.924	888	42	1135	64
784-01	449	0.012759878	0.000572715	9.50722E−06	0.282065852	1.82145E−05	1.867E−11	−15.61	0.64	−0.983	1651	25	2395	40
784-02	444	0.014941723	0.000656861	2.74033E−05	0.282083188	1.45007E−05	1.867E−11	−15.14	0.51	−0.980	1631	20	2361	32
784-03	444	0.007244341	0.000325752	2.47699E−06	0.282091461	1.62149E−05	1.867E−11	−14.75	0.57	−0.990	1605	22	2337	36
784-04	444	0.012185757	0.000552053	1.09464E−05	0.282060657	1.53485E−05	1.867E−11	−15.90	0.54	−0.983	1657	21	2409	34
784-05	446	0.009677837	0.000443517	1.06365E−05	0.282047819	1.67944E−05	1.867E−11	−16.28	0.59	−0.987	1670	23	2434	37
784-06	459	0.011061897	0.000497818	9.03315E−06	0.282072607	1.55347E−05	1.867E−11	−15.13	0.55	−0.985	1639	21	2373	34
784-07	451	0.012163345	0.000518988	4.28045E−06	0.282056956	1.64512E−05	1.867E−11	−15.87	0.58	−0.984	1661	23	2412	36
784-08	453	0.01163659	0.000533395	1.56605E−05	0.282011901	2.94814E−05	1.867E−11	−17.42	1.04	−0.984	1723	40	2511	64
784-09	462	0.012191561	0.000540957	4.63493E−06	0.282072919	1.50907E−05	1.867E−11	−15.07	0.53	−0.984	1640	21	2371	33
784-10	459	0.019191151	0.000843098	1.29082E−05	0.28205033	2.0257E−05	1.867E−11	−16.03	0.72	−0.975	1684	28	2428	44
784-11	445	0.019717756	0.000796717	1.09748E−05	0.282021209	1.65092E−05	1.867E−11	−17.35	0.58	−0.976	1722	23	2500	36
784-12	447	0.015602102	0.000687874	2.31288E−05	0.282072275	1.63988E−05	1.867E−11	−15.47	0.58	−0.979	1647	23	2384	36
784-13	454	0.01835734	0.000794316	2.03602E−05	0.282083617	1.67776E−05	1.867E−11	−14.94	0.59	−0.976	1636	23	2357	37
784-14	450	0.019251858	0.000806768	1.92993E−05	0.282052692	1.48995E−05	1.867E−11	−16.13	0.53	−0.976	1679	21	2428	33
784-15	460	0.013683397	0.00060216	4.71296E−05	0.282086243	1.50861E−05	1.867E−11	−14.66	0.53	−0.982	1624	21	2344	33
791-01	369	0.055971534	0.002260688	4.88834E−05	0.282636509	1.41945E−05	1.867E−11	2.41	0.50	−0.932	902	21	1195	32

Table 4 (*continued*)

Sample no.	t (Ma)	$^{176}Yb/^{177}Hf$	$^{176}Lu/^{177}Hf$	2σ	$^{176}Hf/^{177}Hf$	2σ	λ	$\varepsilon_{Hf}(t)$	2σ	$f_{Lu/Hf}$	T_{DM1}	2σ	T_{DM}^{C}	2σ
791-02	445	0.027177485	0.001142455	3.90253E−05	0.282518009	2.76266E−05	1.867E−11	0.13	0.98	−0.966	1042	39	1400	62
791-03	360	0.007383895	0.000326933	1.13318E−06	0.281391302	1.38322E−05	1.867E−11	−41.38	0.49	−0.990	2553	19	3907	29
791-04	367	0.056678231	0.002309266	3.29873E−05	0.282542251	1.47714E−05	1.867E−11	−0.98	0.52	−0.930	1040	22	1409	33
791-05	367	0.035722391	0.001439959	1.17395E−05	0.282560347	1.23544E−05	1.867E−11	−0.13	0.44	−0.957	990	18	1355	28
791-06	367	0.018876437	0.000760128	8.72397E−06	0.282491019	1.46597E−05	1.867E−11	−2.41	0.52	−0.977	1069	20	1500	33
791-07	364	0.033296672	0.001396543	5.8917E−05	0.282586081	1.15211E−05	1.867E−11	0.73	0.41	−0.958	952	16	1298	26
791-08	365	0.024431884	0.000913192	5.89734E−06	0.282893776	1.52274E−05	1.867E−11	11.76	0.54	−0.972	507	22	593	34
791-09	367	0.013005402	0.000525806	1.40673E−06	0.282514583	1.04157E−05	1.867E−11	−1.52	0.37	−0.984	1030	14	1443	23
794-01	335	0.013536287	0.000604434	3.20307E−05	0.2826597	1.29439E−05	1.867E−11	2.89	0.46	−0.982	830	18	1137	29
794-02	338	0.075679536	0.002993033	0.000191042	0.282677728	1.85131E−05	1.867E−11	3.06	0.66	−0.910	859	28	1129	42
794-03	337	0.028949218	0.001233605	1.10247E−05	0.282678858	1.26494E−05	1.867E−11	3.47	0.45	−0.963	817	18	1102	28
794-04	342	0.036208308	0.001551603	3.45774E−05	0.282660444	1.25846E−05	1.867E−11	2.86	0.45	−0.953	850	18	1145	28
794-05	331	0.037992926	0.001640169	2.61542E−05	0.282665635	1.32811E−05	1.867E−11	2.79	0.47	−0.951	845	19	1141	30
794-06	328	0.047118377	0.001980974	3.49133E−05	0.282674513	1.5734E−05	1.867E−11	2.96	0.56	−0.940	840	23	1127	35
794-07	335	0.038202573	0.001700624	2.09784E−05	0.282605354	1.43006E−05	1.867E−11	0.73	0.51	−0.949	933	21	1275	32
794-08	342	0.02490738	0.001082085	3.16024E−05	0.282672087	1.18676E−05	1.867E−11	3.38	0.42	−0.967	823	17	1112	27
794-09	335	0.03848239	0.001657909	2.99939E−05	0.282638646	1.13854E−05	1.867E−11	1.91	0.40	−0.950	884	16	1200	25
794-10	347	0.027271362	0.001185368	8.10223E−05	0.282645305	2.10911E−05	1.867E−11	2.51	0.75	−0.964	863	30	1171	47
794-11	344	0.019369329	0.000857569	3.95444E−05	0.282637197	1.29006E−05	1.867E−11	2.24	0.46	−0.974	867	18	1186	29
794-12	338	0.037151655	0.001550106	1.52741E−05	0.282634311	1.21803E−05	1.867E−11	1.85	0.43	−0.953	888	17	1206	27
794-13	345	0.021270848	0.000984271	1.35344E−05	0.282652776	1.10654E−05	1.867E−11	2.78	0.39	−0.970	848	16	1152	25
794-14	348	0.03155645	0.001387334	5.77499E−05	0.28263	1.17563E−05	1.867E−11	1.95	0.42	−0.958	890	17	1208	26
794-15	347	0.023456305	0.000985279	4.60891E−05	0.282711907	1.30624E−05	1.867E−11	4.92	0.46	−0.970	765	18	1018	29
797-1-01	350	0.030640517	0.001311166	9.68736E−05	0.282699233	1.60945E−05	1.867E−11	4.46	0.57	−0.961	790	23	1050	36
797-1-02	341	0.112061178	0.004469457	0.000129391	0.282812519	1.94194E−05	1.867E−11	7.56	0.69	−0.865	686	30	844	44
797-1-03	341	0.037131624	0.001589745	1.37674E−05	0.28268338	1.52291E−05	1.867E−11	3.64	0.54	−0.952	818	22	1095	34
797-1-04	339	0.076336167	0.003103622	0.00011439	0.282709632	1.66654E−05	1.867E−11	4.19	0.59	−0.907	814	25	1058	37
797-1-05	349	0.039242716	0.001677547	3.78207E−05	0.282690861	1.48899E−05	1.867E−11	4.05	0.53	−0.949	809	21	1074	33
797-1-06	351	0.031253321	0.001402025	1.20399E−05	0.282606864	1.34697E−05	1.867E−11	1.19	0.48	−0.958	923	19	1259	30
797-1-07	344	0.027894019	0.001191282	3.31671E−05	0.282654425	1.48918E−05	1.867E−11	2.77	0.53	−0.964	851	21	1152	33
797-1-08	341	0.071778713	0.002976161	0.000100839	0.282637096	1.85766E−05	1.867E−11	1.69	0.66	−0.910	919	28	1219	42
797-1-09	341	0.052988418	0.002320417	3.80359E−05	0.282666646	1.5401E−05	1.867E−11	2.88	0.55	−0.930	859	23	1143	35
797-1-10	347	0.04961562	0.002064517	4.48936E−05	0.282627415	1.4308E−05	1.867E−11	1.68	0.51	−0.938	910	21	1224	32
797-1-11	353	0.073482844	0.002952633	1.84946E−05	0.282655004	1.6051E−05	1.867E−11	2.57	0.57	−0.911	892	24	1172	36
797-1-12	344	0.116728666	0.004690995	7.34453E−05	0.282700286	1.82605E−05	1.867E−11	3.59	0.65	−0.859	866	29	1100	41
797-1-13	345	0.041454728	0.001820162	2.54133E−05	0.282667851	1.50743E−05	1.867E−11	3.12	0.53	−0.945	846	22	1131	34
797-1-14	356	0.058092709	0.002349162	0.000147433	0.282681298	1.82282E−05	1.867E−11	3.71	0.65	−0.929	838	27	1102	41
797-1-15	341	0.019694036	0.000833945	1.44471E−05	0.282690088	1.59879E−05	1.867E−11	4.05	0.57	−0.975	792	22	1068	36
798-01	342	0.03120234	0.001327835	1.39013E−05	0.282624305	1.37913E−05	1.867E−11	1.63	0.49	−0.960	896	20	1223	31
798-02	350	0.027463025	0.001138926	7.72886E−05	0.28269298	1.31233E−05	1.867E−11	4.27	0.46	−0.966	795	19	1061	29
798-03	350	0.028404252	0.001233191	2.78453E−05	0.282654258	1.2789E−05	1.867E−11	2.88	0.45	−0.963	852	18	1150	29
798-04	364	0.058917251	0.002366592	5.15088E−05	0.282709499	1.48006E−05	1.867E−11	4.87	0.52	−0.929	797	22	1035	33
798-05	355	0.027174914	0.001199602	6.87939E−06	0.282660082	1.22173E−05	1.867E−11	3.20	0.43	−0.964	843	17	1133	27
798-06	346	0.057876338	0.00234132	2.56086E−05	0.282627761	1.67377E−05	1.867E−11	1.60	0.59	−0.929	916	24	1228	37
798-07	348	0.020584873	0.000885649	3.85643E−05	0.282648243	1.68999E−05	1.867E−11	2.71	0.60	−0.973	852	24	1160	38
798-08	342	0.030408389	0.001287678	1.84501E−05	0.282674965	1.32328E−05	1.867E−11	3.43	0.47	−0.961	824	19	1109	30
798-09	357	0.039020691	0.001621181	3.41987E−05	0.282672618	1.38021E−05	1.867E−11	3.59	0.49	−0.951	834	20	1110	31
798-10	357	0.029665132	0.001274678	3.28116E−05	0.282659757	1.2748E−05	1.867E−11	3.22	0.45	−0.962	845	18	1134	29
798-11	351	0.012532028	0.000556136	1.87532E−05	0.282648206	1.2229E−05	1.867E−11	2.85	0.43	−0.983	845	17	1153	27
798-12	353	0.024143095	0.001032496	2.67556E−05	0.282681793	1.31488E−05	1.867E−11	3.97	0.47	−0.969	808	19	1083	29
798-13	356	0.026206985	0.001144396	1.06034E−05	0.282667098	1.39018E−05	1.867E−11	3.49	0.49	−0.966	832	20	1116	31
798-14	348	0.192771665	0.00780389	0.000190042	0.282717606	1.77259E−05	1.867E−11	3.57	0.63	−0.765	924	31	1105	40
798-15	361	0.054738578	0.002128952	4.39419E−05	0.282617459	1.66222E−05	1.867E−11	1.60	0.59	−0.936	926	24	1240	37
798−2-01	366	0.100912492	0.004280366	8.54683E−05	0.282680754	1.77274E−05	1.867E−11	3.43	0.63	−0.871	886	27	1128	40
798-2-02	368	0.01293909	0.000555949	2.23089E−05	0.282572308	2.12437E−05	1.867E−11	0.54	0.75	−0.983	951	30	1314	47
798-2-03	368	0.076587179	0.003360758	1.70428E−05	0.282701674	1.6805E−05	1.867E−11	4.43	0.59	−0.899	832	25	1066	38
798-2-04	374	0.038803709	0.001682953	9.29662E−05	0.28270143	1.71858E−05	1.867E−11	4.96	0.61	−0.949	794	25	1037	39
798-2-05	383	0.037025211	0.001544156	2.97556E−05	0.282648371	1.48002E−05	1.867E−11	3.31	0.52	−0.953	867	21	1149	33
798-2-06	369	0.033309056	0.001414544	6.59551E−05	0.282668699	1.77734E−05	1.867E−11	3.76	0.63	−0.957	835	25	1109	40
798-2-07	365	0.091159493	0.003747485	6.52577E−05	0.282699696	2.03754E−05	1.867E−11	4.21	0.72	−0.887	844	31	1078	46
798-2-08	359	0.059185547	0.00243061	4.35568E−05	0.282704579	1.6614E−05	1.867E−11	4.57	0.59	−0.927	806	24	1049	37
798-2-09	377	0.02446469	0.000996649	3.60099E−05	0.282659181	1.41745E−05	1.867E−11	3.70	0.50	−0.970	839	20	1119	32
798-2-10	376	0.073529431	0.002873801	2.82402E−05	0.282655582	2.14688E−05	1.867E−11	3.08	0.76	−0.913	889	32	1158	48
798-2-11	371	0.040178051	0.001614392	0.000139489	0.282609885	3.06418E−05	1.867E−11	1.67	1.09	−0.951	924	44	1244	69
798-2-12	371	0.094163098	0.003810209	3.04141E−05	0.282695932	2.26833E−05	1.867E−11	4.18	0.80	−0.885	851	35	1084	51

during our routine analyses, with a weighted mean $^{176}Hf/^{177}Hf$ ratio of 0.282007 ± 0.000007 (2σ, n = 36). It is not distinguishable from a weighted mean $^{176}Hf/^{177}Hf$ ratio of 0.282000 ± 0.000005 (2σ) using a solution analysis method by Morel et al. (2008). A decay constant for ^{176}Lu of 1.867×10^{-11} yr^{-1} (Soderlund et al., 2004) was adopted to calculate initial $^{176}Lu/^{177}Hf$ ratios. The $\varepsilon_{Hf}(t)$ value was calculated by assuming chondritic values of $^{176}Lu/^{177}Hf = 0.282785$ and $^{176}Hf/^{177}Hf = 0.0336$ (Bouvier et al., 2008). The single-stage model age (T_{DM1}) is calculated relative to the depleted mantle with a present-day $^{176}Hf/^{177}Hf = 0.28325$ and $^{176}Lu/^{177}Hf = 0.0384$ (Griffin et al., 2000). The two-stage continental crust model ages (T_{DM}^{C}) are also calculated by plotting the initial $^{176}Hf/^{177}Hf$ of zircons back to the depleted mantle evolutionary curve using the value of $^{176}Lu/^{177}Hf$ (0.015) for the average continental crust (Griffin et al., 2000).

3.3. Geochemistry

Representative samples were crushed and powdered in agate mortars. Major elements were measured by ARL-9800 X-ray fluorescence spectrometer, with analytical precision better than 1%, at the Centre of Modern Analysis in Nanjing University. Trace elements and rare earth elements (REEs) were analyzed by ICP-MS (Finnigan Element II) at the State Key Laboratory for Mineral Deposits Research of Nanjing University, with precision generally better than 10% for most of the analyzed elements. International standards were employed to define the accuracy and precision of analyses throughout the analytical processes for ICP-MS. Detailed analytical procedure is similar to those described by Gao et al. (2003).

4. Results

4.1. Zircon U–Pb geochronology

The typical CL photos of zircons are presented in Fig. 4. The U–Pb dating results are listed in Table 3 and graphically illustrated in Figs. 5 and 6.

4.1.1. Zircons of early Paleozoic granitoids

Zircons separated from sample 784 are euhedral with clear oscillatory zoning (Fig. 4), indicating their magmatic origin. They yield variable abundances of Th (from 67 to 309 ppm), U (from 117 to 405 ppm), and high Th/U ratios (0.47–0.88). A total of 15 analyses yield a weighted mean $^{206}Pb/^{238}U$ age of 450.9 ± 3.3 Ma (MSWD = 0.98; Fig. 5). This age is interpreted as the crystallization age for sample 784.

Zircons from sample 782 are similar with those from sample 784, but show more blurry oscillatory zoning. Variable abundances of Th (from 61 to 910 ppm), U (from 148 to 1376 ppm), and high Th/U ratios (0.41–0.79) are obtained. A total of 14 spots yield a mean $^{206}Pb/^{238}U$ age of 433.8 ± 3.5 Ma (MSWD = 0.23; Fig. 5). This age is interpreted as the crystallization age for sample 782.

Representative zircons separated from sample 766 are euhedral and prismatic with clear oscillatory zoning (Fig. 4), indicative of magmatic origin. The zircons show variable abundances of Th (36–1128 ppm) and U (24–2787 ppm), and high Th/U ratios (from 0.4 to 2.12) in Table 3. Out of the 15 U–Pb analyses, one spot gives young age of 291 Ma, the remaining 14 concordant ages yield a weighted mean $^{206}Pb/^{238}U$ age of 399 ± 3.3 Ma (MSWD = 1.02; Fig. 5) that is considered to represent the crystallization age of sample 766.

4.1.2. Zircons of late Paleozoic granitoids

Zircons of sample 798-2 are prismatic with typical broad oscillatory zoning (Fig. 4), showing very higher Th (249–13,328 ppm) and U (163–2524 ppm), and high Th/U ratios (from 1.23 to 5.28), indicating their magmatic origin. 12 concordant ages yield a weighted mean $^{206}Pb/^{238}U$ age of 370.8 ± 3.9 Ma (MSWD = 1.3; Fig. 5). This age is considered to represent the crystallization age of sample 798-2.

Zircons separated from sample 791 are euhedral and prismatic with clear oscillatory zoning and aspect ratios of 1:2–1:3 (Fig. 4), indicative of magmatic origin. The zircons show Th of 68–345 ppm, U of 132–944 ppm and high Th/U ratios of 0.21–0.97. Out of the 9 U–Pb analyses, one spot gives older age of 445 Ma, the remaining 8 concordant ages yield a weighted mean $^{206}Pb/^{238}U$ age of 365.6 ± 3.5 Ma (MSWD = 0.29; Fig. 6). This latter age is interpreted as the crystallization age of this sample.

Sample 798 was collected from the Alagou region. The similar magmatic features are also displayed in zircons from this sample. The zircons are up to 200 μm in length with aspect ratios of 1:2–1:3, showing variable abundances of Th (63–1180 ppm) and U (85–869 ppm), and high Th/U ratios (from 0.74 to 1.69). Fifteen concordant ages yield a mean $^{206}Pb/^{238}U$ age of 352.2 ± 2.8 Ma (MSWD = 1.15; Fig. 6). This age is considered as the crystallization age of this sample.

Zircons separated from sample 761 are euhedral and prismatic with clear oscillatory zoning (Fig. 4), indicative of magmatic origin. The Th (78–341 ppm), U (111–536 ppm) and high Th/U ratios (from 0.55 to 1.28), as well as clear oscillatory zoning on CL images, favor magmatic origin. 15 analyses with discordance within ±10% yield a weighted mean $^{206}Pb/^{238}U$ age of 351.6 ± 2.9 Ma (MSWD = 0.89; Fig. 6) considered to represent the crystallization age of sample 761.

Sample 797-1 was collected near sample 798. Zircons separated from sample 797-1 are similar to those of sample 797, with clear oscillatory zoning (Fig. 4), indicative of magmatic origin. The concentrations of Th (73–1163 ppm), and U (67–742 ppm) and high Th/U ratios of 0.62–2.1, as well as clear oscillatory zoning on CL photos, are indicative of magmatic origin. A total of 15 spots with discordance within ±10% yield a mean $^{206}Pb/^{238}U$ age of 345.7 ± 2.7 Ma (MSWD = 1; Fig. 6). Thus this age is considered as the crystallization age of sample 797-1.

Zircons separated from sample 794 are typical magmatic origin with clear oscillatory zoning (Fig. 4). The concentrations of Th (71–820 ppm) and U (91–523 ppm) and high Th/U ratios (from 0.57 to 1.66) are consistent with their magmatic origin. Out of the 15 determinations, 14 are near the concordia line, yielding a weighted mean $^{206}Pb/^{238}U$ age of 338.9 ± 3.4 Ma (MSWD = 1.3; Fig. 6). This age is considered as the crystallization age of this sample.

Sample 763 was collected from the Alagou region, too. Typical zircons were separated, with Th of 57–1601 ppm and U of 234–1591 ppm and high Th/U ratios of 0.14–1.60. Out of the 15 determinations, one was performed on inherited core with age of 1452 Ma. The remaining 14 spots are near the concordia line, giving a weighted mean $^{206}Pb/^{238}U$ age of 337 ± 2.9 Ma (MSWD = 0.51; Fig. 6). Thus, this age is interpreted as the crystallization age of this sample.

4.2. Zircon Hf isotopic compositions

All U–Pb dated zircons were chosen for *in-situ* Lu–Hf isotopic analysis. The Hf analyses were performed near the domains used for U–Pb dating spots. In order to discuss the Hf isotopic composition evolution history, the initial $^{176}Hf/^{177}Hf$ values and $\varepsilon_{Hf}(t)$ were compiled using the zircon $^{206}Pb/^{238}U$ ages. The results of the Hf isotopic analyses are given in Table 4, and illustrated in Fig. 7. The $\varepsilon_{Hf}(t)$ values and histograms of Hf model ages (T^C_{DM}) for studied samples are shown in Fig. 8.

Fifteen *in-situ* Lu–Hf analyses were obtained for sample 784. The data show negative $\varepsilon_{Hf}(t)$ values of –17.42 to –14.66 with a mean of −15.72 (Fig. 7), corresponding to T^C_{DM} ages of 2337 to 2511 Ma with a weighted mean age of 2403 Ma (Fig. 8). These results indicate that early Paleoproterozoic crust with an age of ca. 2400 Ma is a major magmatic source for these ~450 Ma zircons.

Zircons from sample 766 show $\varepsilon_{Hf}(t)$ values from −3.69 to 0.76, and the results of samples 791 and 761 are from −2.41 to 2.41 and from −2.04 to 1.75, respectively. Two $\varepsilon_{Hf}(t)$ analyses from sample 791 (−41.38 and 11.76) and one result (−8.67) from sample 761 are excluded due to vastly different values from the other zircons obtained from the same samples. The $\varepsilon_{Hf}(t)$ results of samples 766, 791 and 761 correspond to T^C_{DM} ages of 1300–1500 Ma (Fig. 8). These data are interpreted to reflect the involvement of Mesoproterozoic crustal elements during the emplacement of the Devonian to Early Carboniferous granitoids (~400–350 Ma).

About fifteen zircon Hf analyses were performed for samples 763, 782, 794, 797-1, 798 and 798-2, respectively. In spite of their large span in age (433–337 Ma), some common signatures are noted in these samples. The similar features include positive $\varepsilon_{Hf}(t)$ values, a similar range of $\varepsilon_{Hf}(t)$ values, and a similar range in T^C_{DM} ages (see Table 4). The T^C_{DM} ages range from 844 Ma to 1314 Ma with a peak model age at 1116 Ma. The positive $\varepsilon_{Hf}(t)$ values, indicate that the juvenile addition has played a major contribution to the crustal formation of Central Tianshan in Paleozoic.

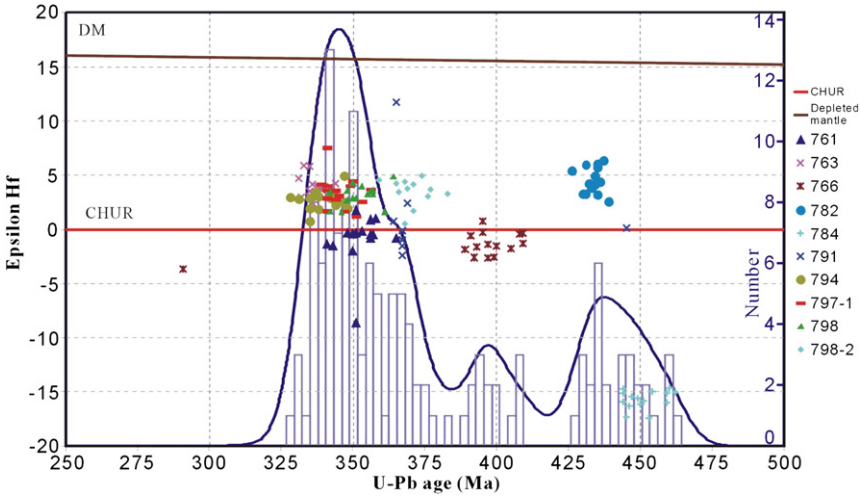

Fig. 7. Epsilon Hf isotopic results and relative U–Pb age probability for zircons from the granitoid rocks in Central Tianshan.

4.3. Major and trace element geochemistry

The analytical results of major and trace element geochemistry are given in Table 5. The samples 763, 766, 782, 791, 794 and 797-1 exhibit SiO_2 contents ranging between 68.5 and 75.6 wt.%, and plot in the granite field in the TAS diagram (Fig. 9a). In contrast, samples 761, 784, 798 and 798-2 yield lower SiO_2 contents of 58.8–62.04 wt.% and plot in the diorite field. As shown in Fig. 9b, nearly all of these samples belong to the metaluminous granitoids with low A/CNK (<1), except samples 794 and 797-1, that are slightly peraluminous as indicated by higher A/CNK ratios (1.02 and 1.03). However, according to the classification diagram (Fig. 9c) of Frost et al. (2001), all these samples plot into the magnesian granitoid field with low FeO^T / (FeO^T + MgO) (0.60–0.69). According to Fig. 9d and e, samples 761, 798 and 798-2 belong to the calc-alkaline affinity, while the remaining other samples plot into the high-K calc-alkaline to shoshonitic fields. However, in the Ce/Yb–Ta/Yb diagram (Fig. 9f), all the studied samples lie within the shoshonitic field.

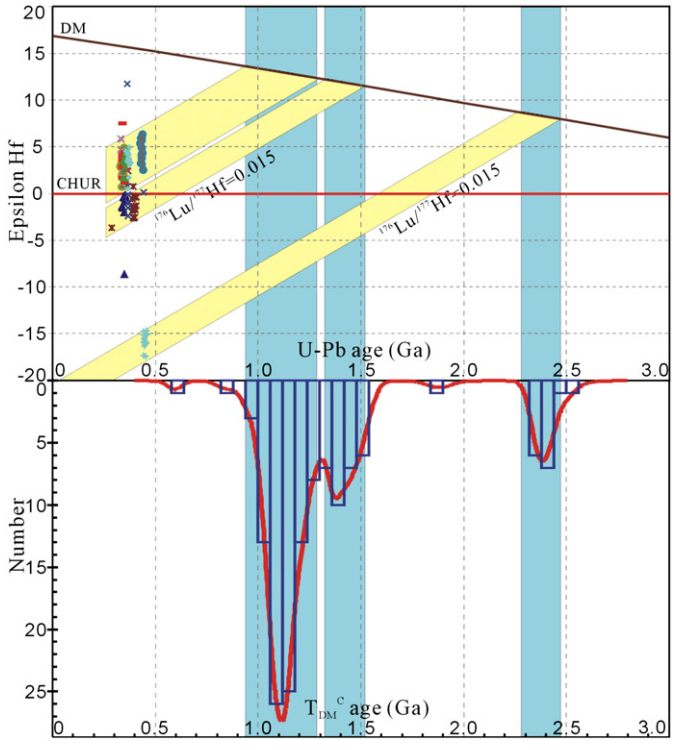

Fig. 8. Epsilon Hf isotopic results and relative Hf model age (T_{DM}^{C}) probability histogram for zircons from the granitoid rocks in Central Tianshan.

The primary striking characteristics of all studied samples is that they yield similar chondrite-normalized steep rare earth element (REE) patterns showing significant enrichment of light rare earth element (LREE) relative to heavy rare earth element (HREE) with high $(La/Yb)_{CN}$ (9.10–29.68) (Fig. 10a and Table 5). With the exception of samples 761, 794 and 797-1, all the remaining samples show distinct negative Eu anomalies.

In the primitive mantle-normalized spider diagrams (Fig. 10b), significant negative Nb, Ta and Ti anomalies are the common feature of all these granitoids, similar to arc granitoids from Brazil (Guimaraes et al., 2011). Except for samples 761, 794, 798 and 798-2, the others exhibit conspicuous depletion in large iron lithophile elements (LILE), such as Ba and Sr. Sample 766 is enriched in Rb, while samples 794 and 798 are Rb depleted.

5. Discussion

5.1. Petrogenesis and tectonic regime of the granitoids in Central Tianshan

5.1.1. The early Paleozoic (ca. 450–400 Ma) granitoids

As mentioned above, the samples 784 (ca. 450 Ma), 782 (ca. 434 Ma) and 766 (ca. 400 Ma) exhibit the petrological and geochemical features of I-type granitoids: high LREE/HREE ratios with high $(La/Yb)_{CN}$ ratios, flat patterns for HREEs, significant negative Eu anomalies, HFSE (Nb, Ta, and Ti) depletion and LILE enrichment, that indicate garnets, titanites, or rutiles are the main residual phases. Geochemically, all these three plutons yield $10^4 \times$ Ga/Al values (2.3–2.5) lower than the value (>2.6) of A-type granitoids (Whalen et al., 1987), and low aluminum saturation index (ASI) of <1 and $FeO^T/(FeO^T + MgO)$ <0.7, which are typical indicators for I-type granitoids. Further evaluation of Zr–SiO_2 discrimination, confirms their distinct I-type affinity (Fig. 11), consistent with their position in the high-K calc-alkaline to shoshonitic field (Fig. 9; Chappell and White, 1983; Roberts and Clemens, 1993).

Chappell and White (1974) consider that I-type granitoids originate from a partial melt of mafic to intermediate metaigneous rocks without any sedimentary contamination. More recent studies (Xiong et al., 2005; Lei et al., 2012) demonstrated that at depths >40 km and pressure >1.2 GPa, mafic crust can melt to generate magmas with high $(La/Yb)_{CN}$ ratios. Kemp et al. (2007) argued that I-type granitoids could be generated by mingling of sedimentary materials and mantle-derived magmas rather than reworking of ancient metaigneous crustal rocks. Recently,

Table 5
Major (wt.%) and trace element (ppm) data for the granitoid rocks from Central Tianshan.

Sample	761	763	763-1	766	782	782-1	784
Name	Granodiorite	K-feldspar granite	K-feldspar granite	K-feldspar granite	K-feldspar granite	K-feldspar granite	Granodiorite
SiO_2	62.04	71.63	72.51	75.55	73.08	73.26	60.4
TiO_2	0.65	0.24	0.22	0.13	0.16	0.15	0.74
Al_2O_3	17.28	14.18	13.29	12.46	12.87	13.49	16.82
Fe_2O_3T	4.7	1.51	1.52	0.9	1.35	1.44	6.11
Fe_2O_3	0.63	0.2	0.21	0.12	0.18	0.2	0.83
FeO	3.6	1.16	1.16	0.69	1.03	1.11	4.68
MnO	0.07	0.03	0.03	0.02	0.02	0.02	0.09
MgO	2.52	0.73	0.63	0.4	0.56	0.59	2.73
CaO	4.92	1.15	1.15	0.49	0.78	0.51	5.75
Na_2O	4.3	4.17	3.78	4.13	3.81	3.94	2.83
K_2O	1.82	4.86	4.72	4.87	5.39	5.47	2.99
P_2O_5	0.18	0.04	0.04	0.02	0.06	0.06	0.15
LOI	1.26	1.58	1.55	0.57	1.23	1	1.45
Total	99.8	100.2	99.5	99.6	99.4	100	100.2
ACNK	0.96	1	0.99	0.96	0.95	1.01	0.92
FeOT	4.23	1.36	1.37	0.81	1.21	1.3	5.5
Li	21.57	4.39	5.24	3.23	2.98	3.05	19.95
Sc	8.5	3.29	3.08	0.76	3.77	3.43	14.96
Ti	3863	1402	1298	765	1075	1100	4943
V	87.14	17.64	19.37	5.29	13.44	13.22	150.4
Cr	27.95	8.07	5.35	2	3.92	4.1	27.77
Mn	498.9	215.5	180.8	114.3	125.6	126.5	679.4
Co	11.49	2.01	1.9	0.38	1.76	1.75	14.61
Ni	9.15	1.27	2.62	4.37	2.03	2.44	10.02
Cu	12.1	3.34	1.82	0.98	2.09	2.01	9.88
Zn	189.5	222.06	47.57	27.84	23.24	26.38	60.46
Ga	22.1	16.53	15.06	16.5	16.5	16.42	21.49
Rb	47.92	168	182.9	136.8	99.96	102.1	102
Sr	460.8	149	108.6	86.11	109.7	120.4	294.6
Y	12.17	22.68	17.96	21.23	18.58	18.07	17.36
Zr	214.7	139.5	132.8	141.1	184.8	191.2	217
Nb	7.17	8.35	7.72	12.17	11.14	10.65	10.54
Mo	0.37	0.4	0.06	0.26	0.15	0.13	0.24
Cd	0.19	0.17	0.09	0.19	0.21	0.2	0.23
Sn	1.51	3.77	4.66	1.05	1.51	1.56	2.16
Cs	2.49	2.33	2.11	0.52	1.45	1.5	2.72
Ba	521.4	543.4	433	208.8	747.6	717	811.5
Hf	5.24	5.17	4.01	5.11	5.4	5.42	5.97
Ta	0.36	1.26	0.89	1.14	0.43	0.44	0.77
W	0.19	1.48	1.29	0.27	0.16	0.12	0.28
Pb	11.45	14.11	13.33	16.49	22.47	22.87	8.18
Bi	0.05	0.16	0.14	0.01	0.02	0.02	0.04
Th	5.58	20.47	14.89	19.83	13.34	13.58	6.23
U	0.75	3.25	2.42	2.04	1.14	1.23	1.87
La	21.43	27.32	23.27	34.21	17.61	22.07	20.13
Ce	37.53	50.3	46.49	66.95	36.56	44.21	43.36
Pr	4.96	6.14	5.27	8.94	4.02	4.98	5.65
Nd	20.54	21.14	19.88	32.05	14.08	17.35	23.6
Sm	3.55	3.67	3.51	6.56	2.95	3.06	4.45
Eu	1.13	0.59	0.5	0.35	0.66	0.61	1.32
Gd	3.22	4.25	3.32	6.2	2.86	3.05	4.28
Tb	0.42	0.64	0.48	0.85	0.44	0.42	0.58
Dy	2.6	4.29	3.28	5.22	3.28	3.12	3.58
Ho	0.57	0.94	0.79	1.03	0.72	0.71	0.7
Er	1.49	2.83	2.19	2.59	2.16	2.06	1.94
Tm	0.2	0.42	0.32	0.31	0.3	0.32	0.3
Yb	1.29	2.79	2.16	1.82	1.81	1.78	1.68
Lu	0.2	0.44	0.33	0.24	0.3	0.29	0.26
TiO_2/Al_2O_3	0.037615741	0.016925247	0.0165538	0.01043339	0.012432	0.0111193	0.0439952
Zr/Al_2O_3	12.42476852	9.837799718	9.992475546	11.3242376	14.358974	14.173462	12.901308
$(La/Yb)_{CN}$	15.54	9.16	10.08	17.58	9.10	11.60	11.21
Zr + Nb + Ce + Y	271.57	220.83	204.97	241.45	251.08	264.13	288.26
Y/Nb	1.69735007	2.716167665	2.32642487	1.74445357	1.6678636	1.6967136	1.6470588
Rb/Zr	0.223195156	1.204301075	1.377259036	0.96952516	0.5409091	0.5339958	0.4700461
Y + Nb	19.34	31.03	25.68	33.4	29.72	28.72	27.9
Yb + Ta	1.65	4.05	3.05	2.96	2.24	2.22	2.45
Ta/Yb	0.279069767	0.451612903	0.412037037	0.62637363	0.2375691	0.247191	0.4583333
Ce/Yb	29.09302326	18.02867384	21.52314815	36.7857143	20.198895	24.837079	25.809524

Hf isotopic compositions have proven to be a useful method to probe magma sources (Hawkesworth and Kemp, 2006; Kemp et al., 2006; Zheng et al., 2006; Kemp et al., 2007; Zheng et al., 2007, 2008).

The $\varepsilon_{Hf}(t)$ values from the granitoids in our study suggest a variety of source regions beneath Central Tianshan. The negative $\varepsilon_{Hf}(t)$ values (mean of −15.72) from sample 784 suggest that the source of the

Table 5 (*continued*)

791	791-1	794	797-1	798	798-1	798-2
K-feldspar granite	K-feldspar granite	Biotite K-feldspar granite	Granite	Granodiorite	Granodiorite	Diorite
71.39	71.02	68.49	72.8	60.5	60.92	58.77
0.32	0.31	0.3	0.2	0.47	0.5	0.93
13.71	13.65	15.92	13.47	18.45	18.57	16.06
1.78	1.72	2.31	1.43	4.24	4.62	6.94
0.24	0.23	0.31	0.19	0.57	0.62	0.94
1.36	1.32	1.77	1.1	3.25	3.54	5.3
0.03	0.03	0.06	0.03	0.06	0.08	0.13
0.71	0.68	1.1	0.64	2.19	2.51	4.17
0.54	0.72	2.76	1.29	5.61	5.4	5.99
4.11	4.21	4.03	3.62	5.1	4.85	3.65
5.62	5.56	3.68	4.42	1.76	1.7	1.33
0.11	0.1	0.1	0.09	0.21	0.23	0.07
0.99	1.02	0.76	1.17	1.5	1.3	2
99.4	99.1	99.7	99.4	100.2	100.8	100.1
0.99	0.96	1.02	1.03	0.9	0.94	0.87
1.6	1.55	2.08	1.29	3.82	4.16	6.24
6.62	10.77	19.79	5.73	7.58	11.79	13.96
4.67	5.95	4.89	2.07	8.54	7.18	27.39
2295	2780	2020	1461	3337	3567	7501
26.61	30.72	43.12	20.24	82.83	95.44	264.5
3.23	4.39	5.89	1.7	14.75	17.89	25.3
249.6	242.4	429.7	203.4	433.2	604.5	1049.8
2.38	2.62	4.4	2.18	9.99	11.6	25.78
2.53	4.1	3.91	1.31	10.36	11.42	12.24
2.53	4.57	1.73	1.9	5.41	5.77	15.62
34.9	45.2	49.1	32.59	56.96	55.51	68.38
18.14	21.18	16.58	16.06	23.31	24.32	23.04
155.2	198.5	57.66	91.78	29.18	38.6	46.09
184.2	203.4	378.3	207.3	653.3	512	535.8
22.58	23.95	10.96	6.73	11.21	12.18	23.08
338.3	347.5	165.9	134.7	240.8	220.2	210
15.44	17.93	5.37	5.74	4.67	5.63	11.04
0.09	0.14	0.14	0.11	0.16	0.11	0.24
0.29	0.19	0.19	0.09	0.26	0.16	0.13
2.28	2.48	1.02	0.64	0.69	0.94	1.73
3.04	3.37	2.23	1.08	0.68	2.32	0.76
945.9	1099.5	1263.9	847.1	717.4	639.9	425.6
8.17	10.49	4.14	4.23	5.94	5.4	5.2
1.08	1.41	0.44	0.37	0.29	0.34	0.7
1.1	1.39	4.4	0.36	0.29	0.28	0.4
36.76	27.58	17.29	20.54	10.81	10.45	9.83
0.16	0.2	0.07	0.04	0.24	0.05	0.04
25.63	27.46	5.92	13.79	5.02	4.73	4.89
2.06	2.94	0.94	0.89	0.86	0.8	0.87
48.59	58.85	26	22.21	22.43	23.19	29.27
99.04	123.33	47.17	39.87	41.38	38.71	68.36
10.55	13.73	4.94	4.07	4.57	4.81	7.83
38.41	49.92	17.69	14.66	16.16	19.28	31.5
6.26	8.14	3	2.13	2.93	3.29	5.65
1.16	1.39	0.99	0.85	1.23	1.37	1.42
5.3	5.74	2.54	1.45	2.45	3.03	4.65
0.7	0.8	0.33	0.18	0.31	0.38	0.63
4.3	4.87	2.28	1.14	2.12	2.29	4.34
0.83	1.03	0.45	0.26	0.41	0.53	0.96
2.54	3.14	1.31	0.73	1.35	1.45	2.62
0.38	0.44	0.19	0.11	0.18	0.21	0.39
2.16	2.59	1.11	0.7	1.19	1.22	2.14
0.35	0.45	0.19	0.14	0.2	0.21	0.32
0.0233406	0.0227106	0.018844221	0.0148	0.0254743	0.0269251	0.0579
24.675419	25.457875	10.42085427	10	13.051491	11.857835	13.076
21.04	21.26	21.91	29.68	17.63	17.78	12.80
475.36	512.71	229.4	187.04	298.06	276.72	312.48
1.4624352	1.3357501	2.040968343	1.1725	2.4004283	2.1634103	2.0906
0.4587644	0.571223	0.34755877	0.6814	0.1211794	0.1752952	0.2195
38.02	41.88	16.33	12.47	15.88	17.81	34.12
3.24	4	1.55	1.07	1.48	1.56	2.84
0.5	0.5444015	0.396396396	0.5286	0.2436975	0.2786885	0.3271
45.851852	47.617761	42.4954955	56.957	34.773109	31.729508	31.944

magma was dominated by reworking of ancient lower crust. In contrast, the positive $\varepsilon_{Hf}(t)$ values (mean ~5) that are shown on zircons from sample 782 support a more juvenile source with limited contributions of older crustal sources. Between these two extremes, sample 766 (ca. 400 Ma) yielded $\varepsilon_{Hf}(t)$ values ranging from −2.6 to +0.76 suggesting that perhaps magmas mixing played a more

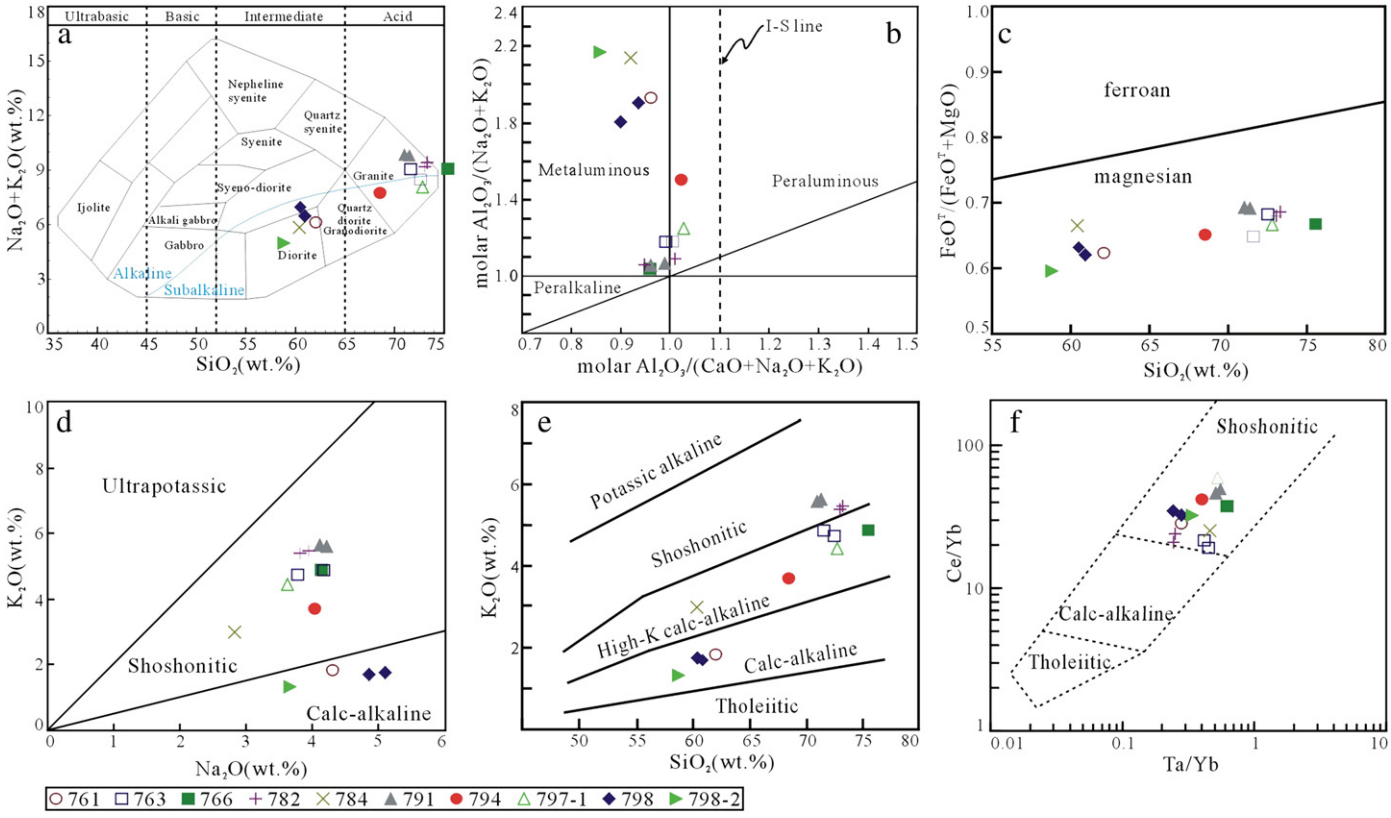

Fig. 9. (a) Total alkalis *vs.* silica diagram (after Wilson, 1989). (b) Shand's index for the granitoids (after Maniar and Piccoli, 1989). (c) The compositional range of the granitoids in the $FeO^T/(FeO^T + MgO)$ *vs.* SiO_2 diagram (after Frost et al., 2001). (d) K_2O–Na_2O diagram (after Peccerillo and Taylor, 1976). (e) K_2O *vs.* SiO_2 (after Peccerillo and Taylor, 1976; Calanchi et al., 2002). (f) Ce/Yb–Ta/Yb diagram (after Müller et al., 1992).

dominant role in the formation of these melts (Kemp et al., 2007; Bolhar et al., 2008).

The tectonic setting for our granitoids can be discerned *via* several different discrimination diagrams. All of the early Paleozoic granitoids plot in the volcanic arc granitoid field and the continental arc field (Fig. 12a–f). The primitive mantle normalized spider diagrams in Fig. 10 indicate negative Nb, Ta and Ti anomalies resembling those of Precambrian Brazilian arc granitoids (Guimaraes et al., 2011). All these discrimination diagrams demonstrate that the early Paleozoic granitoids formed in an active continental margin.

5.1.2. The ca. 370–350 Ma granitoids

Samples 798-2 (ca. 370 Ma), 798 and 798-1 (ca. 352 Ma), 761 (ca. 352 Ma) fall within the diorite field and exhibit typical characteristics of metaluminous and magnesian granitoids (Fig. 9a, b, c). Unlike the early Paleozoic granitoids, these samples lie within the calc-alkaline field in Fig. 9d, e and within the shoshonitic field in Fig. 9f. Sample 791 (ca. 365 Ma) is a typical shoshonitic metaluminous granite. Shoshonitic magmas can be generated in various tectonic regimes, such as within-plate, oceanic arc, continental arc and post-collisional arc (Müller et al., 1992; Qiu et al., 2003) as well as post-orogenic regimes such as the Neoproterozoic Pan-African orogens (Ferré et al., 1998; Bonin et al., 1998), the late Cenozoic Himalaya range (Miller et al., 1999), the Paleozoic West Kunlun belt (Jiang et al., 2002) and the European Tethys (Pe-Piper et al., 2009).

Geochemically, the A-type granitoid characteristics are observed in sample 791 (Fig. 11): the average 10000Ga/Al value >2.6 (Zr + Nb + Ce + Y) of 791 (475 ppm) and 791-1 (512 ppm) greater than 350 ppm, which are the typical indicator of A-type granitoids (Whalen et al., 1987). In addition, these samples are enriched in incompatible trace elements, including LILE and HFSE, but low in compatible elements such as Ba, Sr and Eu (Bonin, 2007). Based on the Y/Nb ratio >1.2 (Table 5), we infer that these A-type rocks formed in post-collisional setting (Eby, 1992). The A-type granitoids are formed under great temperature, sometimes low pressure (generated from the middle-upper crust; Clemens et al., 1986; Patino Douce, 1997).

Although some characteristics of I-type granitoids are exhibited by 798 (and 798-1) and 761 (Figs. 11a, b and 12a–d); we note several paradoxes within the various discrimination diagrams. For example, in Fig. 12f, samples fall in the post-collisional arc field. In the chondrite-normalized REE patterns (Fig. 10a), a significant positive Eu anomaly is shown for these samples that is atypical of I-type granitoids formed in a subduction-related setting (Wu et al., 2003). The positive Eu anomaly could be attributed to the residual amphibole and/or pyroxene. In addition, these rocks show striking depletion of Rb in the trace element spidergram (Fig. 10b). Although these data are somewhat contradictory, we infer that these granitoids (ca. 352 Ma) were most likely formed in a post-collisional setting. In the K_2O–Na_2O and K_2O–SiO_2 diagrams, samples 798-2 (ca. 370 Ma), 798 and 798-1 (ca. 352 Ma), 761 (ca. 352 Ma) fall in the calc-alkaline magmatic field, signifying the maturity and stabilization of the subduction zone (Shervais, 2001) in accord with the post-collisional setting.

5.1.3. The ca. 340 Ma granitoids

The ca. 340 Ma granitoids are weakly peraluminous and fall within the I-type granitoid field (Fig. 11b). Geochemical data demonstrate that these rocks are potassic and fall in the high-K calc-alkaline to shoshonitic field. In southeastern Australia, the average I-type granitoids plot in the high-K field on the K_2O–SiO_2 plot (Chappell and White, 1983). In addition, low Nb and Y contents, and low $FeO^T / (FeO^T + MgO) < 0.7$ indicate that they belong to I-type granitoids (Table 5) consistent with their location within the Zr–SiO_2 diagram (Fig. 11b).

According to the discrimination diagrams of tectonic settings in Fig. 12, these rocks consistently plot into the VAG setting, and have

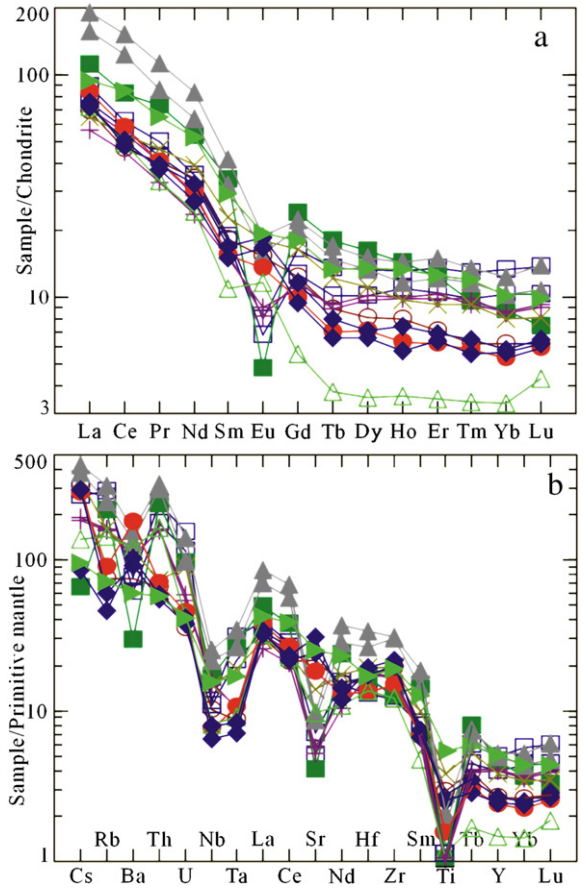

Fig. 10. (a) Chondrite-normalized REE patterns. (b) Primitive mantle-normalized spider diagrams. The values of chondrite and primitive mantle are from Boynton (1984) and Sun and McDonough (1989), respectively.

close affinity to the continental arc. The steep LREE/HREE patterns expressed by the $(La/Yb)_{CN}$ ranging from 9.16 to 29.68 and the depletion in Nb, Ta and Ti (Fig. 10) suggest that these granitoids were probably generated in an Andean-type continental arc.

5.2. Contribution of juvenile materials in Central Tianshan

The granitoids investigated in this study also yield important information regarding the crustal evolution of Central Tianshan. Zircon Hf isotopic compositions reveal that there are three distinct crustal sources involved in the formation of the Paleozoic granitoids (Fig. 8) as evidenced by $\varepsilon_{Hf}(t)$ values and Hf T^{C}_{DM} model ages. The oldest crustal source is suggested by the Hf T^{C}_{DM} model ages of 2337–2511 Ma with a peak of 2403 Ma. The striking negative $\varepsilon_{Hf}(t)$ values (mean −15.7) suggest that this early Paleoproterozoic crust played a key role in the genesis of ~450 Ma granitoids of Central Tianshan. In addition, the Hf T^{C}_{DM} model ages of ~2400 Ma probably indicate an episode of juvenile material addition during global continental crust growth.

A number of the granitoids in this study yielded Hf T^{C}_{DM} model ages of ~1400 Ma (Fig. 8). These zircons show $\varepsilon_{Hf}(t)$ values ranging from −3 to 0, indicating some involvement of ca. 1400 Ma crust during the Paleozoic formation of our studied granitoids.

Models that posit Central Tianshan as part of the Tarim block in the Precambrian are supported by these ~1400 Ma model ages as similar ages are reported from Tarim and its surrounding areas, such as a zircon U–Pb upper intercept age of 1404 ± 18 Ma for a gneiss in East Tianshan (Hu et al., 2001), two weighted SHRIMP zircon U–Pb ages of 1436 ± 13 Ma and 1405.2 ± 7.8 Ma for granodiorites in East Tianshan (Hu et al., 2006), and a granitic gneiss in Bingdaban of Central Tianshan was dated at ca. 1.4 Ga by SHRIMP method (Chen et al., 2009), ages of (1453 ± 15)–(1458 ± 40) Ma by SHRIMP U–Pb for gneissic granites (Shi et al., 2010) and an inherited zircon with age of ~1400 Ma from the Xingxingxia granodiorite (Lei et al., 2011).

Rogers and Santosh (2002) and Zhao et al. (2003, 2004) pointed out that the fragmentation of Columbia commenced at ca. 1.6 Ga ago and persisted until its final dispersal at ca. 1.2 Ga as evidenced by widespread 1.6–1.2 Ga continental rifting, anorogenic magmatism and emplacement of mafic dyke swarms in all cratons of Columbia. Later on, regional-scale large igneous province (LIP) events at 1460, 1380 and 1280 Ma are thought to be related to the breakup of Columbia (Ernst et al., 2008). Although the paleogeography of the Columbia supercontinent is only poorly known (Zhao et al., 2002; Meert, 2012), Tarim is sometimes placed between northern Australia and South China near the NW margin of Laurentia. These ca. 1400 Ma ages may therefore record

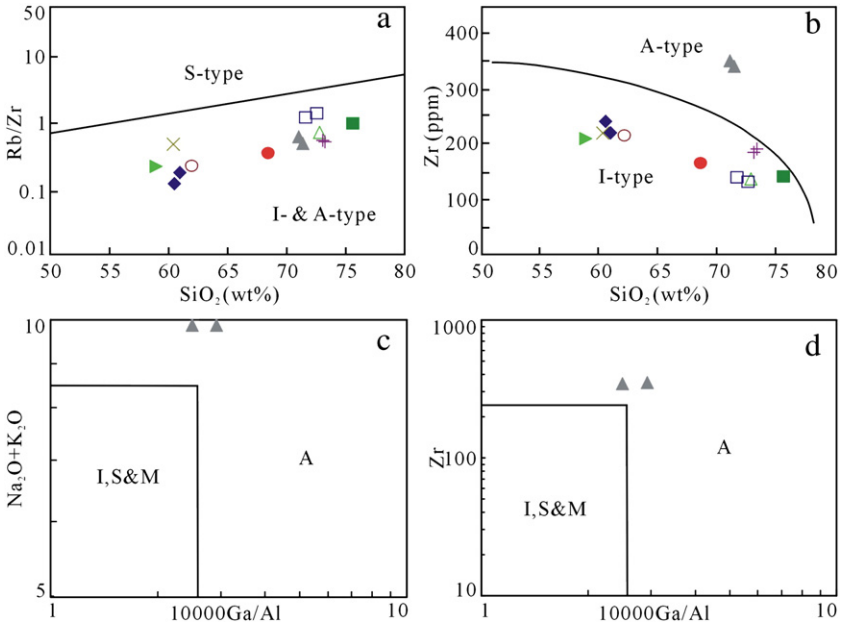

Fig. 11. (a) Rb/Zr–SiO_2 discrimination diagram for I- and A-types granitoids from S-type rocks (Harris et al., 1986). (b) Zr *vs.* SiO_2 discrimination diagram for I-type from A-type granitoid rocks (Collins et al., 1982). (c) $Na_2O + K_2O$ *vs.* 10,000 Ga/Al and (d) Zr *vs.* 10,000 Ga/Al discrimination diagrams of Whalen et al. (1987).

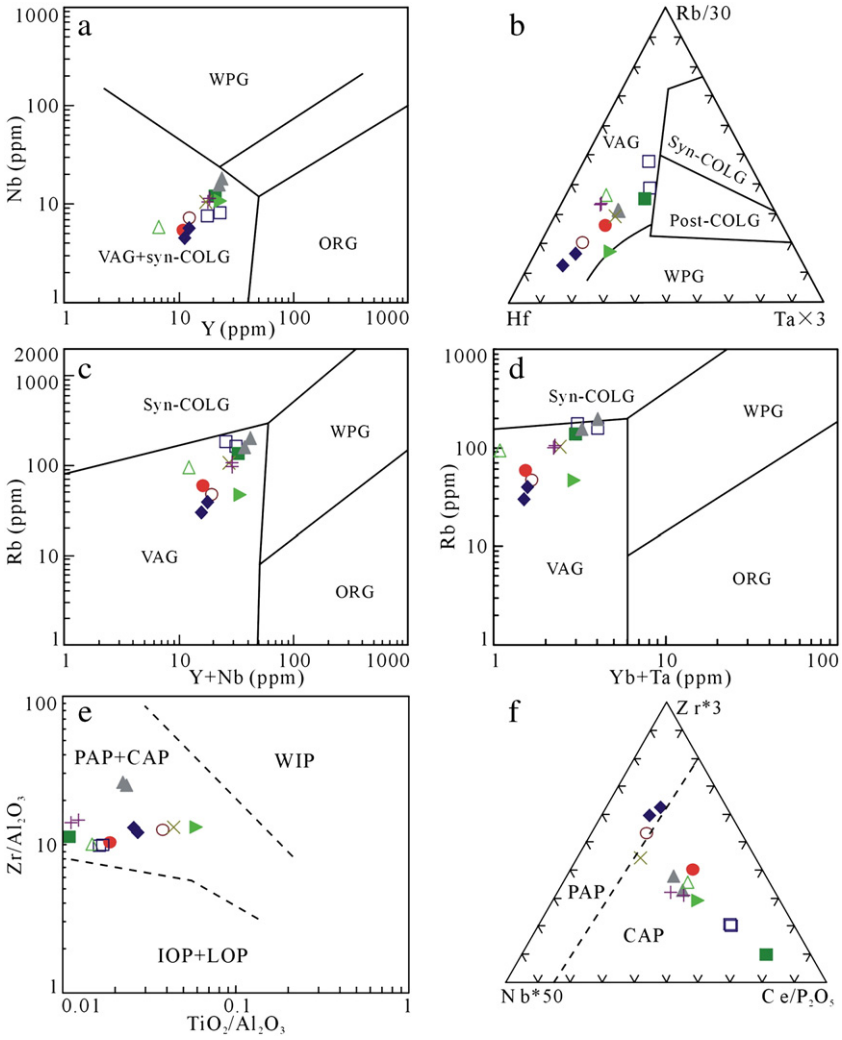

Fig. 12. (a, c and d) Discrimination diagrams of Nb *vs.* Y, Rb *vs.* Y + Nb and Rb *vs.* Yb + Ta (Pearce et al., 1984). (b) Discrimination diagram of Rb/30-Ta × 3-Hf (Harris et al., 1986). (e and f) Discrimination diagrams of Zr/Al_2O_3-TiO_2/Al_2O_3 and Zr^*3–Ce/P_2O_5–Nb^*50 (after Müller et al., 1992). ORG, ocean ridge granitoids; Post-COLG, post-collisional granitoids; Syn-COLG, syn-collisional granitoids; VAG, volcanic arc granitoids; WPG, within-plate granitoids; CAP, continental arc potassic; IOP, initial oceanic arc potassic; LOP, late oceanic arc potassic; PAP, post-collisional arc potassic; WIP, within plate potassic.

the breakup of Columbia in the Tarim craton (Rogers and Santosh, 2009; Meert, 2012).

As shown in Fig. 8, a third component of ancient crust is present in the Paleozoic granitoids of Central Tianshan. This component is characterized by prominent Hf T^C_{DM} model ages ranging from 1200 to 900 Ma with a peak at ca. 1120 Ma. These zircons are also marked by positive $\varepsilon_{Hf}(t)$ values, implying that the juvenile crust plays a key part in the formation of the late Paleozoic magma source and the addition of depleted mantle material to the continental crust at around 1120 Ma. The ages of 1200–900 Ma overlap with so-called "Grenville-ages" of 1300–900 Ma that are thought to correspond with the formation of the Rodinia supercontinent (Hoffman, 1991; Lowman and Gable, 1999; Fitzsimons, 2000; Condie, 2001; Li and Powell, 2001; Wingate et al., 2002; Meert and Torsvik, 2003; Pesonen et al., 2003; Rogers and Santosh, 2003, 2004; Condie, 2004; Li et al., 2008).

Therefore, it is evident that the Tarim block (containing Central Tianshan) may be part of Rodinia, preserving the evidence for the assembly of this Precambrian supercontinent (Li et al., 2008; Shu et al., 2011b). This argument has been supported by the following results in the Tarim block: the 969 ± 6 Ma granite in Altyn (Cowgill et al., 2003); the 1000–900 Ma tightly folded metamorphic rocks, and the 1050–1020 Ma amphibolite-facies metamorphic rock dating by hornblende and biotite ^{40}Ar–^{39}Ar in the SW Tarim (C.L. Zhang et al., 2007); and the notable detrital zircon age peak of 955 Ma between 1070 and 752 Ma (Ma et al., 2012b).

As a noticeable feature, a volume of positive $\varepsilon_{Hf}(t)$ values have been revealed in Fig. 8, implying a fact is set in stone that mantle-derived material has been involved in the formation of the Paleozoic granitoids in Central Tianshan. In other words, as part of the CAOB, the Central Tianshan witnessed the crustal growth event. Based on geochronological and isotopic data, some researchers (Jahn et al., 2000, 2004; Kovalenko et al., 2004) pointed out that the growth of continental crust was very significant in the Phanerozoic CAOB, although Condie (1998) suggested that the continental crust growth has been basically completed in Precambrian.

5.3. An integrated model for the Paleozoic Central Tianshan

5.3.1. The role of the Paleo-Asian Ocean

Based on the aforementioned petrological and geochemical results, combined with the temporal and spatial characteristics of the granitoids, we propose a tentative model (as shown in Fig. 13) for the origin and tectonic regime of the Paleozoic granitoids in Central Tianshan.

From late Neoproterozoic to late Paleozoic, the Paleo-Asian Ocean (or Paleo-Tianshan Ocean) existed between the northern European

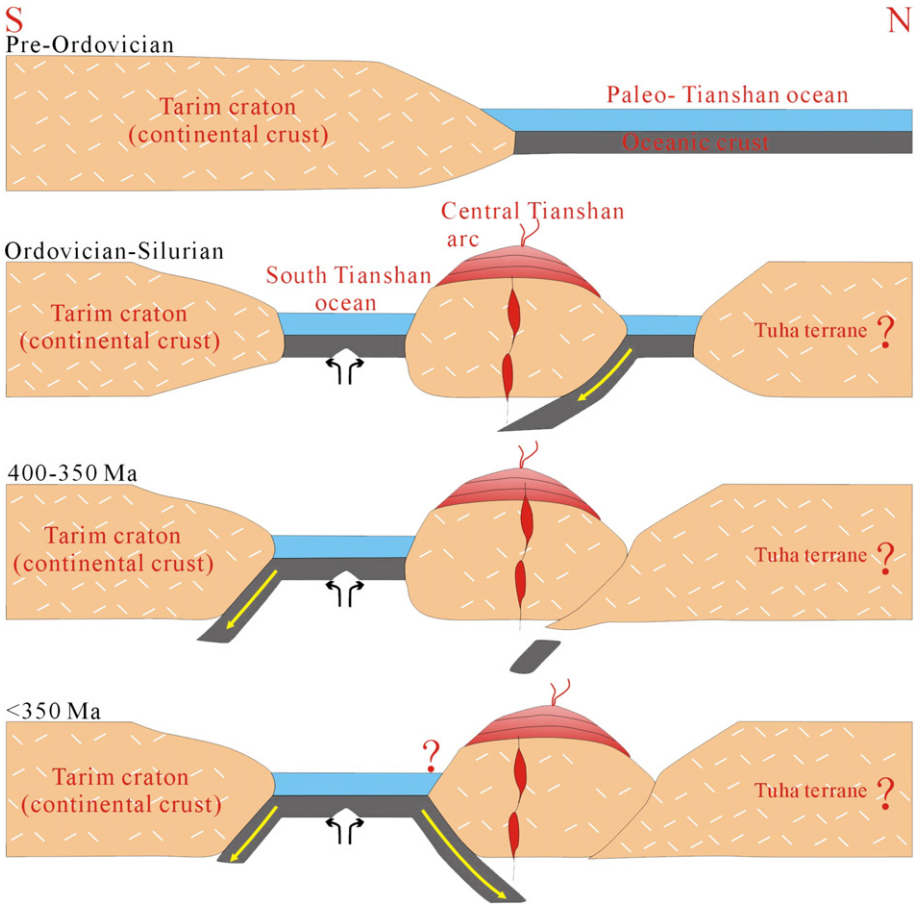

Fig. 13. Geodynamic model of Central Tianshan during Paleozoic (modified from Shu et al., 1998; Wang et al., 2008; Gao et al., 2009; Lin et al., 2009; Charvet et al., 2011; Ge et al., 2012; Ma et al., 2012c).

and Siberian Cratons and the southern Tairm and North China Cratons, similar to the complex archipelago regime of the SW Pacific (Shu et al., 2001; Windley et al., 2007; Xiao et al., 2008; Han et al., 2010). As an archipelago analogous to the present-day western Pacific, the Paleo-Asian Ocean like a natural barrier, distinguished the southern Gondwanian paleogeographic domain (Tarim) and the northern Siberian paleogeographic domain (Filippova et al., 2001; Shu et al., 2002; Windley et al., 2007; Wilhem et al., 2012). And the formation of the CAOB was the derivative product of the final closure of the Paleo-Asian Ocean (Khain et al., 2003; Kheraskova et al., 2003).

Although the exact timing of the final closure of the Paleo-Asian Ocean remains controversial, a commonly used model posits that the northern margin of Tarim (Central Tianshan) was the southernmost part of the CAOB and southward subduction led to the eventual closure of the Paleo-Asian Ocean.

Beginning in the early Paleozoic, the Paleo-Tianshan Ocean began to subduct beneath the northern margin of the Tarim block, leading to the opening of the South Tianshan back-arc basin and isolating the Central Tianshan arc fragment (Fig. 13; Shu et al., 1998; Charvet et al., 2007; Wang et al., 2008; Lin et al., 2009; Charvet et al., 2011). The ubiquitous pre-Carboniferous top-to-the-north shear (indicators such as asymmetric quartz-pressure shadows surrounding a pyrite grain and sigmoidal phenoclasts) and north-verging thrusting and folding preserved in Central Tianshan (Shu et al., 1998; Charvet et al., 2001; Laurent–Charvet et al., 2002; Shu et al., 2002; Laurent-Charvet et al., 2003; Charvet et al., 2004; Shu et al., 2004; Charvet et al., 2007; Wang et al., 2008; Lin et al., 2009; Charvet et al., 2011; Gao et al., 2011; Wang et al., 2011a) are consistent with the assumed southward subduction of the Paleo-Tianshan Ocean.

The Alpine-type ophiolitic suture zone (the Central Tianshan Suture zone) to the north of Central Tianshan represents the closure of the Paleo-Tianshan Ocean. There are a number of ophiolites located along the northern margin of Central Tianshan (in the Weiya, Gangou and Bingdaban areas; Shu et al., 1999; Charvet et al., 2007). The Ordovician–Early Devonian mafic to intermediate volcanic lavas, tuffs and volcanic flysches support the existence of the Central Tianshan arc (Shu et al., 1998) as well as voluminous arc-related granitoids reported in Central Tianshan (Table 2).

Although the ophiolite emplacement provides field evidence for ocean closure, the exact timing and dynamics of the Paleo-Tianshan Ocean closure remains uncertain. Jiang et al. (1999) argued that the closure of the Paleo-Tianshan Ocean occurred in the late Carboniferous. Dong et al. (2011) suggested that southward subduction of the Paleo-Tianshan Ocean beneath Central Tianshan terminated at ~424 Ma. Chen et al. (2012) inferred that the termination of the Paleo-Tianshan Ocean took place in the early Silurian (ca. 440 Ma). Our new data suggest that final closure of the Paleo-Tianshan Ocean most likely occurred between 400 and 350 Ma based on the arc affinity of the 450–400 Ma granitoids and the post-collisional setting for the ca. 350 Ma granitoids.

Based on the high pressure metamorphism observed in Central Tianshan, Shu et al. (2004) argue that the first stage of collision in Central Tianshan occurred during late Silurian to Devonian. The leucogranite is an indicator for the termination of collision, containing muscovite and tourmaline, formed after the primary collision (Chung et al., 2005). Fortunately, a leucogranite from the Central Tianshan was dating to emplace at ca. 354 Ma, indicating that the collision in the northern margin of Central Tianshan must predate 354 Ma (Guo et al., 2007).

5.3.2. The subduction of South Tianshan Ocean beneath Central Tianshan?

Subduction of the Paleo-Tianshan Ocean beneath the Tarim block resulted in the formation of a back-arc basin between Tarim and Central Tianshan during Ordovician–Early Devonian time (South Tianshan Ocean; Shu et al., 1998; Guo et al., 2006; Wang et al., 2008). Following the early closure of the Paleo-Tianshan Ocean triggered by the collision between the Tuha terrane and the Central Tianshan arc (Shu et al., 2002), subduction of the South Tianshan Ocean began.

Two key questions remain controversial regarding the South Tianshan Ocean. The first pertains to the timing of the final closure of the South Tianshan Ocean and the second is in regard the polarity of the subduction zone that resulted in the closure. Southward subduction beneath the Tarim craton was proposed by Shu et al. (1998), Wang et al. (2008) and Charvet et al. (2007) whereas northward subduction was argued by Zhou et al. (2004), L.F. Zhang et al. (2007), Yang and Zhou (2009), Dong et al. (2011), He et al. (2012) and Xiao et al. (2012). An integrated approach (with both north and south facing subduction) was argued by Gao et al. (2009) and Ge et al. (2012).

Southward subduction was argued on the basis of kinematic analyses observed in the Chinese Central and Southern Tianshan areas (such as Shu et al., 1998; Charvet et al., 2007; Wang et al., 2008; Lin et al., 2009; Charvet et al., 2011; Wang et al., 2011a). In the Kumux ophiolitic area, lines of kinematic structural evidence such as asymmetric quartz pressure-shadows and sigmoidal quartz phenoclasts indicate top-to-the-north sense of shear. Prior to the Carboniferous unconformity, the structures (such as fold and thrust) are ubiquitously north verging in the Central Tianshan region (Charvet et al., 2007, 2011). According to the top-to-the-north kinematic analyses of the high pressure (HP) metamorphic rocks and its underlying gneiss (Gao et al., 1995), in combination with the Ordovician–Silurian magmatic arc located south of the HP metamorphic unit in the western Tianshan belt (Wang et al., 2008), Wang et al. (2011a) advocated an intense deformation that took place in deep crustal level during southward subduction of the South Tianshan Ocean. In addition, ca. 420 Ma magmatism in the northern Tarim block reported by Ge et al. (2012) likely occurred in an Andean-type continental arc to further support southward subduction of the South Tianshan Ocean in the early Paleozoic.

As discussed above, the first stage of collision along the northern margin of Central Tianshan between the Tuha terrane and the Central Tianshan arc occurred during 400–350 Ma (also see Shu et al., 1998, 2003; Guo et al., 2006). Therefore the subduction setting did not exist after 350 Ma in the northern margin of Central Tianshan. However, the ca. 340 Ma granitoids of this study exhibited the characteristics of subduction-related I-type granitoid rocks and formed in an active continental margin arc regime. How to explain this geological phenomenon? The northward subduction of the South Tianshan Ocean beneath the Central Tianshan probably could fit it. In addition, according to the 392 ± 7 Ma (SHRIMP zircon method) metamorphic age of the granulite facies ophiolite in Yushugou and 360 ± 2 Ma (glaucophane $^{40}Ar/^{39}Ar$) blueschist in Tonghuashan along the northern margin of the Southern Tianshan belt, Zhou et al. (2004) inferred the existence of the northward subduction of the South Tianshan Ocean. However, until recently, no definite kinematic marks are reported in this region that could be used to indicate the existence of northward subduction of South Tianshan Ocean beneath the Central Tianshan.

From the late Silurian, the Tuha continental block collided with the northern margin of the Central Tianshan arc. The Paleo-Tianshan Ocean rollback to the Karamaili-Yiwu suture zone, evidenced by the southern Gondwana-type assemblage of Cambrian–Ordovician limestone including Agnostus, Ordovician mudstone including Sinoceras and Silurian shale including graptolite, and the northern Siberian-type assemblage of Ordovician mudstone including Isotelus and upper Silurian sandstone including Tuvaella (Shu et al., 2002). Charvet et al. (2007) suggested that the Northern Tianshan belt comprises Carboniferous clastic sedimentary rocks and andesites, and could be a volcanic arc. So, the residual Paleo-Tianshan Ocean probably continued to subduct southward beneath the Tianshan belt, led to the formation of the Northern Tianshan volcanic arc consisting of voluminous andesites, and furthermore large amount of I-type granitoid intrusions (at ca. 340 Ma) in the Central Tianshan arc.

So, the ca. 340 Ma subduction-related I-type granitoids in Central Tianshan may be related to the northward subduction of the South Tianshan Ocean or the on-going southward subduction of the residual Paleo-Tianshan Ocean. The specific formation setting of the ca. 340 Ma granitoids remains an issue. However, at least from ca. 340 Ma, with the early closure of the Paleo-Asian Ocean and/or the beginning of the northward subduction of the South Tianshan Ocean, the Central Tianshan has completed its transition from the Gondwanian paleogeographical domain to be part of the CAOB, which in turn marked the formation of the main architecture of the CAOB.

6. Concluding remarks

(1) Due to the southward subduction of the Paleo-Tianshan Ocean beginning in the early Paleozoic, voluminous I-type granitoids were formed in the Central Tianshan arc. The collision along the northern margin of Central Tianshan occurred at ca. 400–350 Ma.
(2) The outcrops of ca. 340 Ma granitoids in Central Tianshan, formed in an active continental margin arc regime. Their formation was likely related to the northward subduction of the South Tianshan Ocean or the subsequent southward subduction of the residual Paleo-Tianshan Ocean.
(3) The reworking of early Paleoproterozoic (ca. 2400 Ma) crust played an important role in magma genesis of the ca. 450 Ma granitoid intrusion in Central Tianshan.
(4) Mesoproterozoic crust of ~1400 and 1100 Ma can be identified using Hf-isotopic data within the granitoids of Central Tianshan, but a significant amount of juvenile material was generated during the emplacement of the 430–340 Ma granitoids.
(5) Our model for Central Tianshan posits that this region was originally part of the Tarim craton. A tentative tectonic model for Central Tianshan is outlined.

Acknowledgments

We are indebted to Prof. Koen de Jong and two anonymous reviewers for their valuable comments, which have greatly improved our paper. Profs. Ma Yingjun and Wang Baolin are thanked for their support during our field work. Thanks are due to Dr. Zhu Xiaoqing, Yao Jinlong, Chen Xiaoyong and Lin Anjun, for giving a kind help during the zircon U–Pb–Hf isotopic analyses. This research was financially funded by a Foundation for the Author of National Excellent Doctoral Dissertation of PR China (FANEDD, No. 201130), the National Basic Research Program of China (973 Program, No. 2007CB411301), Doctoral training foundation of the Ministry of Education in China (Grant No. 20120091110024), the State Key Laboratory for Mineral Deposits Research of Nanjing University (No. 2008-I-01), and the China Scholarship Council (201206190049).

References

Allen, M.B., Windley, B.F., Zhang, C., 1992. Paleozoic collisional tectonics and magmatism of the Chinese Tien Shan, central Asia. Tectonophysics 220, 89–115.
Biske, Yu.S., Seltmann, R., 2010. Paleozoic Tian-Shan as a transitional region between the Rheic and Urals–Turkestan oceans. Gondwana Research 17, 602–613.
Bolhar, R., Weaver, S.D., Whitehouse, M.J., Palin, J.M., Woodhead, J.D., Cole, J.W., 2008. Sources and evolution of arc magmas inferred from coupled O and Hf isotope systematics of plutonic zircons from the Cretaceous Separation Point Suite (New Zealand). Earth and Planetary Science Letters 268, 312–324.
Bonin, B., 2007. A-type granites and related rocks: evolution of a concept, problems and prospects. Lithos 97, 1–29.
Bonin, B.L., Azzouni-Sekkal, A., Bussy, F., Ferrag, S., 1998. Alkali-calcic and alkaline post-orogenic (PO) granite magmatism: petrologic constraints and geodynamic setting. Lithos 45, 45–70.

Bouvier, A., Vervoort, J.D., Patchett, P.J., 2008. The Lu–Hf and Sm–Nd isotopic composition of CHUR: constraints from unequilibrated chondrites and implications for the bulk composition of terrestrial planets. Earth and Planetary Science Letters 273, 48–57.
Boynton, W.V., 1984. Geochemistry of the rare earth elements: meteorite studies. In: Henderson, P. (Ed.), Rare Earth Element Geochemistry. Elsevier, Amsterdam, pp. 63–114.
Brookfield, M.E., 2000. Geological development and Phanerozoic crustal accretion in the western segment of the southern Tien Shan (Kyrgyzstan, Uzbekistan and Tajikistan). Tectonophysics 328, 1–14.
Calanchi, N., Peccerillo, A., Tranne, C.A., Lucchini, F., Rossi, P.L., Kempton, P., Barbieri, M., Wu, T.W., 2002. Petrology and geochemistry of volcanic rocks from the island of Panarea: implication for mantle evolution beneath the Aeolian island arc (southern Tyrrhenian sea). Journal of Volcanology and Geothermal Research 115, 367–395.
Chappell, B.W., White, A.J.R., 1974. Two contrasting granite types. Pacific Geology 8, 173–174.
Chappell, B.W., White, A.J.R., 1983. Granitoid types and their distribution in the Lachlan Fold Belt, southeastern Australia. Geological Society of Australia Memoir 159, 21–34.
Charvet, J., Laurent-Charvet, S., Shu, L.S., Ma, R.S., 2001. Paleozoic continental accretions in Central Asia around Junggar Block: new structural and geochronological data. Gondwana Research 4, 590–592.
Charvet, J., Laurent-Charvet, S., Shu, L.S., Lu, H.F., Cluzel, D., Faure, M., Wang, B., 2004. Paleozoic geodynamic evolution of Tianshan orogenic belt (NW China): welding of Tarim and Junggar continental blocks. 32nd IGC-Florence, Symposium G05-09 Tethys Reconstruction (Abstract v., abs. 155–3).
Charvet, J., Shu, L.S., Laurent-Charvet, S., 2007. Paleozoic structural and geodynamic evolution of eastern Tianshan (NW China): welding of the Tarim and Junggar plates. Episodes 30, 162–186.
Charvet, J., Shu, L.S., Laurent-Charvet, S., Wang, B., Faure, M., Cluzel, D., Chen, Y., de Jong, K., 2011. Paleozoic tectonic evolution of the Tianshan belt, NW China. Science in China Series D: Earth Sciences 54, 166–184.
Che, Z.C., Liu, H.F., Liu, L., 1994. Formation and Evolution of the Middle Tianshan Orogenic Belt. Geological Publishing House, Beijing 1–135.
Chen, C.M., Lu, H.F., Jia, D., Cai, D.S., Wu, S.M., 1999. Closing history of the southern Tianshan oceanic basin, western China: an oblique collisional orogeny. Tectonophysics 302, 23–40.
Chen, X.Y., Wang, Y.J., Sun, L.H., Fan, W.M., 2009. Zircon SHRIMP U–Pb dating of the granitic gneisses from Bingdaban and Laerdundaban (Tianshan Orogen) and their geological significances. Geochimica 38, 424–431 (in Chinese with English abstract).
Chen, Y.B., Zhang, G.W., Liu, X.M., Xiong, X.L., Yuan, C., Chen, L.L., 2012. Zircons LA-ICP-MS U–Pb dating on the Baluntai deformed granitoids, Central Tianshan Block, northwest China, and its tectonic implications. Geological Review 58, 117–125.
Chu, N.C., Taylor, R.N., Chavagnac, V., Nesbitt, R.W., Boella, R.M., Milton, J.A., German, C.R., Bayon, G., Burton, K., 2002. Hf isotope ratio analysis using multi-collector inductively coupled plasma mass spectrometry: an evaluation of isobaric interference corrections. Journal of Analytical Atomic Spectrometry 17, 1567–1574.
Chung, S.L., Chu, M.F., Zhang, Y., 2005. Tibetan tectonic evolution inferred from spatial and temporal variations in post-collisional magmatism. Earth-Science Reviews 68, 173–196.
Clemens, J.D., Holloway, J.R., White, A.J.R., 1986. Origin of an A-type granite: experimental constraints. American Mineralogist 71, 317–324.
Coleman, R.G., 1989. Continental growth of northwest China. Tectonics 8, 621–635.
Collins, W.J., Beams, S.D., White, A.J.R., Chappell, B.W., 1982. Nature and origin of A-type granites with particular reference to southeastern Australia. Contributions to Mineralogy and Petrology 80, 189–200.
Collins, A.Q., Degtyarev, K.E., Levashova, N.M., Bazhenov, M.L., Van der Voo, R., 2003. Early Paleozoic paleomagnetism of East Kazakhstan: implications for paleolatitudinal drift of tectonic elements within the Ural–Mongol belt. Tectonophysics 377, 229–247.
Condie, K.C., 1998. Episodic continental growth and supercontinents: a mantle avalanche connection? Earth and Planetary Science Letters 163, 97–108.
Condie, K.C., 2001. Mantle Plumes and Their Record in Earth history. Cambridge University Press, Cambridge, UK 305.
Condie, K.C., 2004. Supercontinents and superplume events: distinguishing signals in the geologic record. Physics of the Earth and Planetary Interiors 146, 319–323.
Cowgill, E., Yin, A., Harrison, T.M., Wang, X.F., 2003. Reconstruction of the Altyn Tagh fault based on U–Pb geochronology: role of back thrusts, mantle sutures, and heterogeneous crustal strength in forming the Tibetan Plateau. Journal of Geophysical Research 108 (B7), 2346.
de Jong, K., Xiao, W.J., Windley, B.F., Masago, H., Lo, C.H., 2006. Ordovician $^{40}Ar/^{39}Ar$ phengite ages from the blueschist-facies Ondor Sum subduction-accretion complex (Inner Mongolia) and implications for the early Paleozoic history of continental blocks in China and adjacent areas. American Journal of Science 306, 799–845.
Dong, Y.P., Zhang, G.W., Neubauer, F., Liu, X.M., Hauzenberger, C., Zhou, D.W., Li, W., 2011. Syn- and post-collisional granitoids in the Central Tianshan orogen: geochemistry, geochronology and implications for tectonic evolution. Gondwana Research 20, 568–581.
Eby, G.N., 1992. Chemical subdivision of the A-type granitoids: petrogenetic and tectonic implications. Geology 20, 641–644.
Ernst, R.E., Wingate, M.T.D., Buchan, K.L., Li, Z.X., 2008. Global record of 1600–700 Ma Large Igneous Provinces (LIPs): implications for the reconstruction of the proposed Nuna (Columbia) and Rodinia supercontinents. Precambrian Research 160, 159–178.
Ferré, E.C., Caby, R., Peucat, J.J., Capdevila, R., Monie, P., 1998. Pan-African, post-collisional, ferro-potassic granite and quartz-monzonite plutons of Eastern Nigeria. Lithos 45, 255–279.
Filippova, I.B., Bush, V.A., Didenko, A.N., 2001. Middle Paleozoic subduction belts: the leading factor in the formation of the Central Asian fold-and-thrust belt. Russian Journal of Earth Sciences 3, 405–426.
Fitzsimons, I.C.W., 2000. Grenville-age basement provinces in East Antarctica: evidence for three separate collisional orogens. Geology 28, 879–882.
Frost, B.R., Barnes, C.G., Collins, W.J., Arculus, R.J., Ellis, D.J., Frost, C.D., 2001. A geochemical classification for granitic rocks. Journal of Petrology 42, 2033–2048.
Gao, J., Klemd, R., 2003. Formation of HP-LT rocks and their tectonic implications in the western Tianshan Orogen, NW China: geochemical and age constraints. Lithos 66, 1–22.
Gao, J., He, G.Q., Li, M.S., Xiao, X.C., Tang, Y.Q., 1995. The mineralogy, petrology, metamorphic PTt trajectory and exhumation mechanism of blueschists, south Tianshan, northwestern China. Tectonophysics 250, 151–168.
Gao, J., Li, M.S., Xiao, X.C., Tang, Y.Q., He, G.Q., 1998. Paleozoic tectonic evolution of the Tianshan Orogen, northwestern China. Tectonophysics 287, 213–231.
Gao, J.F., Lu, J.J., Lai, M.Y., Lin, Y.P., Pu, W., 2003. Analysis of trace elements in rock samples using HR-ICP-MS. Journal of Nanjing University (Natural Sciences) 39, 844–850 (in Chinese with English abstract).
Gao, J., Long, L.L., Klemd, R., Qian, Q., Liu, D.Y., Xiong, X.M., Su, W., Liu, W., Wang, Y.T., Yang, F.Q., 2009. Tectonic evolution of the South Tianshan orogen and adjacent regions, NW China: geochemical and age constraints of granitoid rocks. International Journal of Earth Science 98, 1221–1238.
Gao, J., Klemd, R., Qian, Q., Zhang, X., Li, J.L., Jiang, T., Yang, Y.Q., 2011. The collision between the Yili and Tarim blocks of the Southwestern Altaids: geochemical and age constraints of a leucogranite dike crosscutting the HP-LT metamorphic belt in the Chinese Tianshan Orogen. Tectonophysics 499, 118–131.
Ge, R.F., Zhu, W.B., Wu, H.L., Zheng, B.H., Zhu, X.Q., He, J.W., 2012. The Paleozoic northern margin of the Tarim Craton: passive or active? Lithos 142–143, 1–15.
Griffin, W.L., Pearson, N.J., Belousova, E., Jackson, S.E., van Achterbergh, E., O'Reilly, S.Y., Shee, S.R., 2000. The Hf isotope composition of cratonic mantle: LAM-MC-ICPMS analysis of zircon megacrysts in kimberlites. Geochimica at Cosmochimica Acta 64, 133–147.
Griffin, W.L., Belousova, E.A., Shee, S.R., Pearson, N.J., O'Reilly, S.Y., 2004. Archean crustal evolution in the northern Yilgarn Craton: U–Pb and Hf–isotope evidence from detrital zircons. Precambrian Research 131, 231–282.
Gu, L.X., Yang, H., 1990. Rb–Sr geochronology and the tectonic evolution of the east section of the Middle Tianshan Mountains. Journal of Guilin College of Geology 10, 49–55 (in Chinese).
Guimaraes, I.P., Silva Filho, A.F., Almeida, C.N., Macambira, M.B., Armstrong, R., 2011. U–Pb SHRIMP data constraints on calc-alkaline granitoids with 1.3–1.6 Ga Nd T_{DM} model ages from the central domain of the Borborema province, NE Brazil. Journal of South American Earth Sciences 31, 383–396.
Guo, Z.J., Shi, H.Y., Zhang, Z.C., 2006. The tectonic evolution of the south Tianshan paleo-oceanic crust inferred from the spreading structures and Ar–Ar dating of the Hongliuhe ophiolite, NW China. Acta Petrologica Sinica 22, 95–102 (in Chinese with English abstract).
Guo, Z.J., Han, B.F., Zhang, Z.C., Deng, S.T., Liu, C., 2007. The discovery of Paleozoic leucogranite in eastern segment of Chinese Middle Tianshan and its tectonic implications. Acta Petrologica Sinica 23, 1841–1846 (in Chinese with English abstract).
Han, B.F., He, G.Q., Wu, T.R., Li, H.M., 2004. Zircon U–Pb dating and geochemical features of early Paleozoic granites from Tianshan, Xinjiang: implications for tectonic evolution. Xinjiang Geology 22, 4–11 (in Chinese with English abstract).
Han, B.F., Guo, Z.J., Zhang, Z.C., Zhang, L., Chen, J.F., Song, B., 2010. Age, geochemistry, and tectonic implications of a late Paleozoic stitching pluton in the North Tian Shan suture zone, western China. GSA Bulletin 122, 627–640.
Han, B.F., He, G.Q., Wang, X.C., Guo, Z.J., 2011. Late Carboniferous collision between the Tarim and Kazakhstan–Yili terranes in the western segment of the South Tian Shan Orogen, Central Asia, and implications for the Northern Xinjiang, western China. Earth-Science Reviews 109, 74–93.
Harris, N.B.W., Pearce, J.A., Tindle, A.G., 1986. Geochemical characteristics of collision-zone magmatism. In: Coward, M.P., Ries, A.C. (Eds.), Collision Tectonics: Geological Society, London, Special Publication, 19, pp. 67–81.
Hawkesworth, C.J., Kemp, A.I.S., 2006. Using hafnium and oxygen isotopes in zircons to unravel the record of crustal evolution. Chemical Geology 226, 144–162.
He, Z.Y., Zhang, Z.M., Zong, K.Q., Wang, W., Yu, F., 2012. Zircon geochronology of Xingxingxia quartz dioritic gneisses: implications for the tectonic evolution and Precambrian basement affinity of Chinese Tianshan orogenic belt. Acta Petrologica Sinica 28, 1857–1874 (in Chinese with English abstract).
Hendrix, M.S., Graham, S.A., Carroll, A.R., Sobel, E.R., McKnight, C.L., Schulein, B.J., Wang, Z.X., 1992. Sedimentary record and climatic implications of recurrent deformation in the Tianshan: evidence from Mesozoic strata of the north Tarim, south Junggar, and Turpan basins, northwest China. Geological Society of America Bulletin 104, 53–79.
Hoffman, P.F., 1991. Did the breakout of Laurentia turn Gondwanaland inside out? Science 252, 1409–1412.
Hou, K.J., Li, Y.H., Zou, T.R., Qu, X.M., Shi, Y.R., Xie, G.Q., 2007. Laser ablation-MC-ICP-MS technique for Hf isotope microanalysis of zircon and its geological applications. Acta Petrologica Sinica 23, 2595–2604 (in Chinese with English abstract).
Hu, A.Q., Jahn, B.M., Zhang, G.X., Chen, Y.B., Zhang, Q.F., 2000. Crustal evolution and Phanerozoic crustal growth in northern Xinjiang: Nd isotopic evidence. Part I. Isotopic characterization of basement rocks. Tectonophysics 328, 15–51.
Hu, A.Q., Zhang, G.X., Chen, Y.B., Zhang, Q.F., 2001. A model of division of the continental crust basement and the time scales of the major geological events in the Xinjiang-based on studies of isotopic geochronology and geochemistry. Xinjiang Geology 19, 12–19 (in Chinese with English abstract).
Hu, A.Q., Wei, G.J., Deng, W.F., Zhang, J.B., Chen, L.L., 2006. 1.4 Ga SHRIMP U–Pb age for zircons of granodiorite and its geological significance from the eastern segment of the Tianshan Mountains, Xinjiang, China. Geochimica 35, 333–345 (in Chinese with English abstract).
Hu, A.Q., Wei, G.J., Zhang, J.B., Deng, W.F., Chen, L.L., 2007. SHRIMP U–Pb age for zircons of East Tianhu granitic gneiss and tectonic evolution significance from the eastern

Tianshan Mountains, Xinjiang, China. Acta Petrologica Sinica 23, 1795–1802 (in Chinese with English abstract).
Huang, G., Jia, Z.K., Li, H.M., Wang, X.L., Guo, J., 2012. Early Ordovician arc magmatite in Central Tianshan: evidences of geochronology and geochemical on granitic gneiss from Sangshuyuanzi area. Xinjiang Geology 30, 243–252 (in Chinese with English abstract).
Jahn, B.M., Wu, F., Chen, B., 2000. Massive granitoid generation in Central Asian: Nd isotope evidence and implication for continental growth in the Phanerozoic. Episodes 23, 82–92.
Jahn, B.M., Natal'in, B.A., Windley, B.F., Dobretsov, N., 2004. Phanerozoic continental growth in Central Asia. Journal of Asian Earth Sciences 23, 599–603.
Jiang, C.Y., Mu, Y.M., Bai, K.Y., Zhao, X.N., Zhang, H.B., Hei, A.Z., 1999. Chronology, petrology, geochemistry and tectonic environment of granitoids in the southern Tianshan Mountain, western China. Acta Petrologica Sinica 15, 298–308 (in Chinese with English abstract).
Jiang, Y.H., Jiang, S.Y., Ling, H.F., Zhou, X.R., Rui, X.J., Yang, W.Z., 2002. Petrology and geochemistry of shoshonitic plutons from the western Kunlun orogenic belt, Xinjiang, northwestern China: implications for granitoid geneses. Lithos 63, 165–187.
Kelty, T.K., Yin, A., Dash, B., Gehrels, G.E., Ribeiro, A.E., 2008. Detrital-zircon geochronology of Paleozoic sedimentary rocks in the Hangay–Hentey basin, north-central Mongolia: implications for the tectonic evolution of the Mongol–Okhotsk Ocean in Central Asia. Tectonophysics 451, 290–311.
Kemp, A.I.S., Hawkesworth, C.J., Paterson, B.A., Kinny, P.D., 2006. Episodic growth of the Gondwana supercontinent from hafnium and oxygen isotopes in zircon. Nature 439, 580–583.
Kemp, A.I.S., Hawkesworth, C.J., Foster, G.L., Paterson, B.A., Woodhead, J.D., Hergt, J.M., Gray, C.M., Whitehouse, M.J., 2007. Magmatic and crustal differentiation history of granitic rocks from hafnium and oxygen isotopes in zircon. Science 315, 980–983.
Khain, E.V., Bibikova, E.V., Salnikova, E.B., Kröner, A., Gibsher, A.S., Didenko, A.N., Degtyarev, K.E., Fedotova, A.A., 2003. The Palaeo-Asian ocean in the Neoproterozoic and early Palaeozoic: new geochronologic data and palaeotectonic reconstructions. Precambrian Research 122, 329–358.
Kheraskova, T.N., Didenko, A.N., Bush, V.A., Volozh, Y.A., 2003. The Vendian–Early Paleozoic history of the continental margin of eastern Paleogondwana, Paleoasian ocean, and Central Asian foldbelt. Russian Journal of Earth Sciences 5, 165–184.
Klemd, R., Brocker, M., Hacker, B.R., Gao, J., Gans, P., Wemmer, K., 2005. New age constraints on the metamorphic evolution of the high-pressure/low-temperature belt in the western Tianshan Mountains, NW China. Journal of Geology 113, 157–168.
Kovalenko, V.I., Yarmolyuk, V.V., Kovach, V.P., Kotov, A.B., Kozakov, I.K., Salnikova, E.B., Larin, A.M., 2004. Isotopic provinces, mechanism of generation and sources of the continental crust in the Central Asian mobile belt: geological and isotopic evidence. Journal of Asian Earth Sciences 23, 605–627.
Kröner, A., Windley, B.F., Badarch, G., Tomurtogoo, O., Hegner, E., Jahn, B.M., Gruschka, S., Khain, E.V., Demoux, A., Wingate, M.T.D., 2007. Accretionary growth and crust-formation in the Central Asian Orogenic Belt and comparison with the Arabian–Nubian shield. Geological Society of America Memoirs 200, 181–209.
Laurent-Charvet, S., Charvet, J., Monié, P., Shu, L.S., 2003. Late Paleozoic strike-slip shear zones in eastern Central Asia (NW China): new structural and geochronological data. Tectonics 22, 1099–1101.
Laurent–Charvet, S., Charvet, J., Shu, L.S., Ma, R.S., Lu, H.F., 2002. Palaeozoic late collisional strike–slip deformations in Tianshan and Altay, Eastern Xinjiang, NW China. Terra Nova 14, 249–256.
Lei, R.X., Wu, C.Z., Gu, L.X., Zhang, Z.Z., Chi, G.X., Jiang, Y.H., 2011. Zircon U–Pb chronology and Hf isotope of the Xingxingxia granodiorite from the Central Tianshan zone (NW China): implications for the tectonic evolution of the southern Altaids. Gondwana Research 20, 582–593.
Lei, R.X., Wu, C.Z., Chi, G.X., Chen, G., Gu, L.X., Jiang, Y.H., 2012. Petrogenesis of the Palaeoproterozoic Xishankou pluton, northern Tarim block, northwest China: implications for assembly of the supercontinent Columbia. International Geology Review. http://dx.doi.org/10.1080/00206814.2012.678045.
Levashova, N.M., Meert, J.G., Gibsher, A.S., Bazhenov, M.L., 2011. The origin of the Central Asian orogenic belt microcontinents: constrains from paleomagnetism and geochronology. Precambrian Research 185, 37–54.
Li, C.Y., 1981. Frame of plate tectonics, China. Journal of Chinese Geological Academy of Sciences 2, 1–15 (in Chinese).
Li, J.Y., 2006. Permian geodynamic setting of Northeast China and adjacent regions: closure of the Paleo-Asian Ocean and subduction of the Paleo-Pacific Plate. Journal of Asian Earth Sciences 26, 207–224.
Li, Z.X., Powell, C.McA., 2001. An outline of the palaeogeographic evolution of the Australasian region since the beginning of the Neoproterozoic. Earth-Science Reviews 53, 237–277.
Li, W.P., Wang, T., Li, J.B., Kang, X., Yu, F.S., Han, Q.J., Ma, Z.P., 2001. The U–Pb age of zircon from late Caledonian granitoids in Hongliuhe area, east Tianshan mountains, Northwest China and its geological implications. Acta Geoscientia Sinica 22, 231–235 (in Chinese with English abstract).
Li, Z.X., Bogdanova, S.V., Collins, A.S., Davidson, A., De Waele, B., Ernst, R.E., Fitzsimons, I.C.W., Fuck, R.A., Gladkochub, D.P., Jacobs, J., Karlstrom, K.E., Natapovm, L.M., Lu, S., Natapov, L.M., Pease, V., Pisarevsky, S.A., Thrane, K., Vernikovsky, V., 2008. Assembly, configuration, and break-up history of Rodinia: a synthesis. Precambrian Research 160, 179–210.
Li, Q.G., Liu, S.W., Song, B., 2009. Late Mesoproterozoic to Paleozoic tectonothermal events in the eastern segment of the Central Tianshan tectonic zone of Northwestern China: constraints from SHRIMP zircon geochronology. Earth Science Frontiers 16, 175–184 (in Chinese with English abstract).
Lin, W., Faure, M., Shi, Y.H., Wang, Q.C., Li, Z., 2009. Palaeozoic tectonics of the south-western Chinese Tianshan: new insights from a structural study of the high-pressure/low-temperature metamorphic belt. International Journal of Earth Sciences 98, 1259–1274.
Lowman, J.P., Gable, C.W., 1999. Thermal evolution of the mantle following continental aggregation in 3D convection models. Geophysical Research Letters 26, 2649–2652.
Ma, R.S., Wang, C.Y., Ye, S.F., 1993. Tectonic Framework and Crustal Evolution of Eastern Tianshan Mountains. Publishing House of Nanjing University, Nanjing 1–225.
Ma, X.X., Shu, L.S., Jahn, B.M., Zhu, W.B., Faure, M., 2012a. Precambrian tectonic evolution of Central Tianshan, NW China: constraints from U–Pb dating and in situ Hf isotopic analysis of detrital zircons. Precambrian Research 222–223, 450–473.
Ma, X.X., Shu, L.S., Santosh, M., Li, J.Y., 2012b. Detrital zircon U–Pb geochronology and Hf isotope data from Central Tianshan suggesting a link with the Tarim Block: implications on Proterozoic supercontinent history. Precambrian Research 206–207, 1–16.
Ma, X.X., Shu, L.S., Santosh, M., Li, J.Y., 2012c. Petrogenesis and tectonic significance of an early Palaeozoic mafic-intermediate suite of rocks from the Central Tianshan, northwest China. International Geology Review. http://dx.doi.org/10.1080/00206814.2012.727575.
Maniar, P.D., Piccoli, P.M., 1989. Tectonic discrimination of granitoids. Geological Society of America Bulletin 101, 635–643.
Meert, J.G., 2012. What's in a name? The Columbia (Paleopangaea/Nuna) supercontinent. Gondwana Research 21, 987–993.
Meert, J.G., Torsvik, T.H., 2003. The making and unmaking of a supercontinent: Rodinia revisited. Tectonophysics 375, 261–288.
Miller, C., Schuster, R., Klotzli, U., Frank, W., Purtscheller, F., 1999. Post-collisional potassic and ultrapotassic magmatism in SW Tibet: geochemical and Sr–Nd–Pb–O isotopic constraints for mantle source characteristics and petrogenesis. Journal of Petrology 40, 1399–1424.
Morel, M.L.A., Nebel, O., Nebel-Jacobsen, Y.J., Miller, J.S., Vroon, P.Z., 2008. Hafnium isotope characterization of the GJ-1 zircon reference material by solution and laser-ablation MC-ICPMS. Chemical Geology 255, 231–235.
Müller, D., Rock, N.M.S., Groves, D.I., 1992. Geochemical discrimination between shoshonitic and potassic volcanic rocks in different tectonic settings: a pilot study. Mineralogy and Petrology 46, 259–289.
Patino Douce, A.E., 1997. Generation of metaluminous A-type granites by low-pressure melting of calc-alkaline granitoids. Geology 25, 743–746.
Pearce, J.A., Harris, N.B.W., Tindle, A.G., 1984. Trace element discrimination diagrams for the tectonic interpretation of granitic rocks. Journal of Petrology 25, 956–983.
Peccerillo, R., Taylor, S.R., 1976. Geochemistry of Eocene calcalkaline volcanic rocks from the Kastamonu area, northern Turkey. Contributions to Mineralogy and Petrology 58, 63–81.
Peng, M.X., Zhong, C.G., Zuo, Q.H., Zhu, W.M., Yang, S.W., Huang, X., 2012. The formation age and their geological significance of gneissose granites neighbouring Kawabulake area in East Tianshan Mountain. Xinjiang Geology 30, 12–18 (in Chinese with English abstract).
Pe-Piper, G., Piper, D.J.W., Koukouvelas, I., Dolansky, L.M., Kokkalas, S., 2009. Postorogenic shoshonitic rocks and their origin by melting underplated basalts: the Miocene of Limnos, Greece. Geological Society of America Bulletin 121, 39–54.
Pesonen, L.J., Elming, S.A., Mertanen, S., Pisarevsky, S., D'Agrella-Filho, M.S., Meert, J.G., Schmidt, P.W., Abrahamsen, N., Bylund, G., 2003. Palaeomagnetic configuration of continents during the Proterozoic. Tectonophysics 375, 289–324.
Qiu, J.S., Xu, X.S., Jiang, S.Y., 2003. Deep subduction of crust materials and its implication to the genesis of potash-rich volcanic rocks. Earth Science Frontiers 10, 191–200 (in Chinese with English abstract).
Roberts, M.P., Clemens, J.D., 1993. Origin of high-potassium, calc-alkaline, I-type granitoids. Geology 21, 825–828.
Rogers, J.J.W., Santosh, M., 2002. Configuration of Columbia, a Mesoproterozoic supercontinent. Gondwana Research 5, 5–22.
Rogers, J.J.W., Santosh, M., 2003. Supercontinents in Earth History. Gondwana Research 6, 357–368.
Rogers, J.J.W., Santosh, M., 2004. Continents and Supercontinents. Oxford University Press (289 pp.).
Rogers, J.J.W., Santosh, M., 2009. Tectonics and surface effects of the supercontinent Columbia. Gondwana Research 15, 373–380.
Rojas-Agramonte, Y., Kroner, A., Demoux, A., Xia, X., Wang, W., Donskaya, T., Liu, D., Sun, M., 2011. Detrital and xenocrystic zircon ages from Neoproterozoic to Paleozoic arc terranes of Mongolia: significance for the origin of crustal fragments in the Central Asian Orogenic Belt. Gondwana Research 19, 751–763.
Seltmann, S., Shatov, V.V., Yakubchuk, S., 2003. Mineral Deposit Map of Central Asia. Natural History Museum, London, UK, London.
Sengör, A.M.C., Natal'in, B.A., 1996. Paleotectonics of Asia: fragments of a synthesis. In: Yin, A. (Ed.), The Tectonic Evolution of Asia. Cambridge University Press, Cambridge, pp. 486–640.
Sengör, A.M.C., Natal'in, B.A., Burtman, U.S., 1993. Evolution of the Altaid tectonic collage and Paleozoic crustal growth in Eurasia. Nature 364, 209–304.
Shervais, J.W., 2001. Birth, death, and resurrection: the life cycle of suprasubduction zone ophiolites. Geochemistry, Geophysics, Geosystems 2.
Shi, Y.R., Liu, D.Y., Zhang, Q., Jian, P., Zhang, F.Q., Miao, L.C., 2007. SHRIMP zircon U–Pb dating of the Gangou granitoids, Central Tianshan Mountains, Northwest China and tectonic significances. Chinese Science Bulletin 52, 1507–1516.
Shi, W.X., Liao, Q.A., Hu, Y.Q., Yang, Z.F., 2010. Characteristics of Mesoproterozoic granites and their geological significances from Middle Tianshan Block, East Tianshan District, NW China. Geological Science and Technology Information 29, 29–37 (in Chinese with English abstract).
Shu, L.S., Charvet, J., Ma, R.S., 1998. Study of a large scale Paleozoic dextral strike-slip ductile shear zone along the northern margin of the Central Tianshan, Xinjiang. Xinjiang Geology 16, 326–336 (in Chinese with English abstract).

Shu, L.S., Charvet, J., Guo, L., Lu, H.F., 1999. A large-scale Paleozoic dextral ductile strike-slip zone: the Aqqikkudug-Weiya zone along the northern margin of the Central Tianshan belt, Xinjiang, NW China. Acta Geologica Sinica 73, 148–162.
Shu, L.S., Lu, H.F., Yin, D.H., Ma, R.S., Charvet, J., Laurent-Charvet, S., 2001. Late Paleozoic continental accretionary tectonics in northern Xinjiang. Xinjiang Geology 19, 59–63 (in Chinese with English abstract).
Shu, L.S., Charvet, J., Lu, H.F., Laurent-Charvet, S., 2002. Paleozoic accretion–collision events and kinematics of ductile deformation in the eastern part of the Southern-Central Tianshan Belt, China. Acta Geologica Sinica 76, 308–323.
Shu, L.S., Lu, H.F., Yin, D.H., Wang, B., 2003. Paleozoic accretion–collision events and kinematics of ductile deformation in the Central-Southern Tianshan belt. Journal of Nanjing University (Natural Sciences) 39, 17–30 (in Chinese with English abstract).
Shu, L.S., Yu, J.H., Charvet, J., Laurent-Charvet, S., Sang, H.Q., Zhang, R.G., 2004. Geological, geochronological and geochemical features of granulites in the Eastern Tianshan, NW China. Journal of Asian Earth Sciences 24, 25–41.
Shu, L.S., Wang, B., Zhu, W.B., Guo, Z.J., Charvet, J., Zhang, Y., 2011a. Timing of initiation of extension in the Tianshan, based on structural, geochemical and geochronological analyses of bimodal volcanism and olistostrome in the Bogda Shan (NW China). International Journal of Earth Sciences 100, 1647–1663.
Shu, L.S., Deng, X.L., Zhu, W.B., Ma, D.S., Xiao, W.J., 2011b. Precambrian tectonic evolution of the Tarim Block, NW China: new geochronological insights from the Quruqtagh domain. Journal of Asian Earth Sciences 42, 774–790.
Soderlund, U., Patchett, P.J., Vervoort, J.D., Isachsen, C.E., 2004. The ^{176}Lu decay constant determined by Lu–Hf and U–Pb isotope systematics of Precambrian basic intrusions. Earth and Planetary Science Letters 219, 311–324.
Sun, S.S., McDonough, W.F., 1989. Chemical and isotopic systematics of oceanic basalts: implications for mantle composition and processes. In: Saunders, A.D., Norry, M.J. (Eds.), Magmatism in the Ocean Basins: Geological Society, London, Special Publications, 42, pp. 313–345.
Wang, D.G., Zhang, X.M., Fu, H.X., 2006. SHRIMP U–Pb dating of zircons from the north Xiaoyanchi monzodiorite, East Tianshan, Xinjiang, China. Geological Bulletin of China 25, 966–968 (in Chinese with English abstract).
Wang, B., Chen, Y., Zhan, S., Shu, L.S., Faure, M., Cluzel, D., Charvet, J., Laurent-Charvet, S., 2007a. Primary Carboniferous and Permian paleomagnetic results from the Yili Block (NW China) and their implications on the geodynamic evolution of Chinese Tianshan Belt. Earth and Planetary Science Letters 263, 288–308.
Wang, B., Shu, L.S., Cluzel, D., Faure, M., Charvet, J., 2007b. Geochemical constraints on Carboniferous volcanic rocks of the Yili Block (Xinjiang, NW China): implication for the tectonic evolution of Western Tianshan. Journal of Asian Earth Sciences 29, 148–159.
Wang, B., Faure, M., Shu, L.S., Cluzel, D., Charvet, J., de Jong, K., Chen, Y., 2008. Paleozoic tectonic evolution of the Yili Block, Western Chinese Tianshan. Bulletin de la Société Géologique de France 179, 483–490.
Wang, B., Faure, M., Shu, L.S., de Jong, K., Charvet, J., Cluzel, D., Jahn, B.M., Chen, Y., Ruffet, G., 2010a. Structural and geochronological study of high-pressure metamorphic rocks in the Kekesu section (Northwestern China): implications for the late Paleozoic tectonics of the Southern Tianshan. Journal of Geology 118, 59–77.
Wang, X.L., Jiang, S.Y., Dai, B.Z., 2010b. Melting of enriched Archean subcontinental lithospheric mantle: evidence from the ca. 1760 Ma volcanic rocks of the Xiong'er Group, southern margin of the North China Craton. Precambrian Research 182, 204–216.
Wang, B., Shu, L.S., Faure, M., Jahn, B.M., Cluzel, D., Charvet, J., Chung, S.L., Meffre, S., 2011a. Paleozoic tectonics of the southern Chinese Tianshan: insights from structural, chronological and geochemical studies of the Heiyingshan ophiolitic melange (NW China). Tectonophysics 497, 85–104.
Wang, B., Jahn, B.M., Lo, C.H., Shu, L.S., Wu, C.Y., Li, K.S., Wang, F., 2011b. Structural analysis and ^{40}Ar/^{39}Ar thermochronology of Proterozoic rocks in Sailimu area (NW China): implication to polyphase tectonics of the North Chinese Tianshan. Journal of Asian Earth Sciences 42, 839–853.
Wang, X.J., Wang, G.H., Zhuan, S.P., Li, G.D., Wang, D.Q., Wu, L.H., 2011c. Late Ordovician collision and orogen in middle Tianshan: evidences of geochemical analyses and geochronology on metamorphosed granitoid rocks. Acta Petrologica Sinica 27, 2203–2212 (in Chinese with English abstract).
Whalen, J.B., Currie, K.L., Chappell, B.W., 1987. A-type granites: geochemical characteristics, discrimination and petrogenesis. Contributions to Mineralogy and Petrology 95, 407–419.
Wilhem, C., Windley, B.F., Stampfli, G.M., 2012. The Altaids of Central Asia: a tectonic and evolutionary innovative review. Earth-Science Reviews 113, 303–341.
Wilson, M., 1989. Igneous Petrogenesis–A global Tectonic Approach. Unwin Hyman, London 466.
Windley, B.F., Allen, M.B., Zhang, C., Zhao, Z.Y., Wang, G.R., 1990. Paleozoic accretion and Cenozoic red formation of the Chinese Tianshan range, central Asia. Geology 18, 128–131.
Windley, B.F., Alexeiev, D., Xiao, W.J., Kroner, A., Badarch, G., 2007. Tectonic models for accretion of the central Asian orogenic belt. Journal of the Geological Society of London 164, 31–47.
Wingate, M.T.D., Pisarevsky, S.A., Evans, D.A.D., 2002. Rodinia connections between Australia and Laurentia: no SWEAT, no AUSWUS? Terra Nova 14, 121–128.
Wu, F.Y., Jahn, B.M., Wilde, S.A., Lo, C.H., Yui, T.F., Lin, Q., Ge, W.C., Sun, D.Y., 2003. Highly fractionated I-type granites in NE China (I): geochronology and petrogenesis. Lithos 66, 241–273.
Wu, F.Y., Yang, Y.H., Xie, L.W., Yang, J.H., Xu, P., 2006. Hf isotopic compositions of the standard zircons and baddeleyites used in U–Pb geochronology. Chemical Geology 234, 105–126.
XBGMR (Xinjiang Bureau of Geology and Mineral Resources), 1993. Regional Geology of Xinjiang Uygur Autonomous Region. Geological Publishing House, Beijing 841 (in Chinese with English abstract).
XBGMR (Xinjiang Bureau of Geology and Mineral Resources), 1992. Geological map of Xinjiang Uygur Autonomous Region (scale 1: 1500000). Beijing, Geological Publishing House (in Chinese).
Xiao, W.J., Windley, B.F., Hao, J., Zhai, M.G., 2003. Accretion leading to collision and the Permian Solonker suture, Inner Mongolia, China: termination of the central Asian orogenic belt. Tectonics 22, 1069.
Xiao, W.J., Zhang, L.C., Qin, K.Z., Sun, S., Li, J.L., 2004. Paleozoic accretionary and collisional tectonics of the Eastern Tianshan (China): implication for the continental growth of central Asia. American Journal of Science 304, 370–395.
Xiao, W.J., Han, C.M., Yuan, C., Sun, M., Lin, S.F., Chen, H.L., Li, Z.L., Li, J.L., Sun, S., 2008. Middle Cambrian to Permian subduction-related accretionary orogenesis of Northern Xinjiang, NW China: implications for the tectonic evolution of central Asia. Journal of Asian Earth Sciences 32, 102–117.
Xiao, W.J., Windley, B.F., Han, C.M., Yuan, C., Sun, M., Li, J.L., Sun, S., 2009. End Permian to mid-Triassic termination of the southern Central Asian Orogenic Belt. International Journal of Earth Sciences 98, 1189–1217.
Xiao, W.J., Huang, B., Han, C., Li, J., 2010. A review of the western part of the Altaids: a key to understanding the architecture of accretionary orogens. Gondwana Research 18, 253–273.
Xiao, W.J., Windley, B.F., Allen, M.B., Han, C.M., 2012. Paleozoic multiple accretionary and collisional tectonics of the Chinese Tianshan orogenic collage. Gondwana Research 23, 1316–1341. http://dx.doi.org/10.1016/j.gr.2012.01.012.
Xiong, X.L., Adam, J., Green, T.H., 2005. Rutile stability and rutile/melt HFSE partitioning during partial melting of hydrous basalt: implications for TTG genesis. Chemical Geology 218, 339–359.
Xu, X.W., Ma, T.L., Sun, L.Q., Cai, X.P., 2003. Characteristics and dynamic origin of the large-scale Jiaoluotage ductile compressional zone in the eastern Tianshan Mountains, China. Journal of Structural Geology 25, 1901–1915.
Xu, X.Y., Ma, Z.P., Xia, Z.C., Xia, L.Q., Li, X.M., Wang, L.S., 2006. TIMS U–Pb isotopic dating and geochemical characteristics of Paleozoic granitic rocks from the middle-western section of Tianshan. Northwestern Geology 39, 50–75 (in Chinese with English abstract).
Yakubchuk, A., 2004. Architecture and mineral deposit settings of the Altaid orogenic collage: a revised model. Journal of Asian Earth Sciences 23, 761–779.
Yang, S.H., Zhou, M.F., 2009. Geochemistry of the 430-Ma Jingbulake mafic-ultramafic intrusion in Western Xinjiang, NW China: implications for subduction related magmatism in the South Tianshan orogenic belt. Lithos 113, 259–273.
Yang, T.N., Li, J.Y., Sun, G.H., Wang, Y.B., 2006. Earlier Devonian active continental arc in Central Tianshan: evidence of geochemical analyses and zircon SHRIMP dating on mylonitized granitic rock. Acta Petrologica Sinica 22, 41–48 (in Chinese with English abstract).
Yang, T.N., Wang, Y., Li, J.Y., Sun, G.H., 2007. Vertical and horizontal strain partitioning of the Central Tianshan (NW China): evidence from structures and ^{40}Ar/^{39}Ar geochronology. Journal of Structural Geology 29, 1605–1621.
Zhang, C.L., Lu, S.N., Yu, H.F., Ye, H.M., 2007a. Tectonic evolution of the Western Kunlun orogenic belt in northern Qinghai-Tibet Plateau: evidence from zircon SHRIMP and LA-ICP-MS U–Pb geochronology. Science in China Series D: Earth Sciences 50, 825–835.
Zhang, L.F., Ai, Y.L., Li, X.P., Rubatto, D., Song, B., Williams, S., Song, S.G., Ellis, D., Liou, J.G., 2007b. Triassic collision of western Tianshan orogenic belt, China: evidence from SHRIMP U–Pb dating of zircon from HP/UHP eclogitic rocks. Lithos 96, 266–280.
Zhao, G.C., Cawood, P.A., Wilde, S.A., Sun, M., 2002. Review of global 2.1-1.8 Ga orogens: implications for a pre-Rodinia supercontinent. Earth-Science Review 59, 125–162.
Zhao, G.C., Sun, M., Wilde, S.A., Li, S.Z., 2003. Assembly, accretion and breakup of the Paleo-Mesoproterozoic Columbia supercontinent: records in the North China Craton. Gondwana Research 6, 417–434.
Zhao, G.C., Sun, M., Wilde, S.A., Li, S.Z., 2004. A Paleo-Mesoproterozoic supercontinent: assembly, growth, and breakup. Earth-Science Reviews 67, 91–123.
Zheng, Y.F., Zhao, Z.F., Wu, Y.B., Zhang, S.B., Liu, X.M., Wu, F.Y., 2006. Zircon U–Pb age, Hf and O isotope constraints on protolith origin of ultrahigh-pressure eclogite and gneiss in the Dabie orogen. Chemical Geology 231, 135–158.
Zheng, Y.F., Zhang, S.B., Zhao, Z.F., Wu, Y.B., Li, X.H., Li, Z.X., Wu, F.Y., 2007. Contrasting zircon Hf and O isotopes in the two episodes of Neoproterozoic granitoids in South China: implications for growth and reworking of continental crust. Lithos 96, 127–150.
Zheng, Y.F., Wu, R.X., Wu, Y.B., Zhang, S.B., Yuan, H.L., Wu, F.Y., 2008. Rift melting of juvenile arc-derived crust: geochemical evidence from Neoproterozoic volcanic and granitic rocks in the Jiangnan Orogen, South China. Precambrian Research 163, 351–383.
Zhou, D.W., Su, L., Jian, P., Wang, R.S., Liu, X.M., Lu, G.X., Wang, J.L., 2004. The SHRIMP zircon U–Pb age and tectonic implication for the high pressure granulite in the Yushugou ophiolitic terrane of the Southern Tianshan belt. Chinese Science Bulletin 49, 1411–1415 (in Chinese).
Zhu, Y.F., Song, B., 2006. Petrology and SHRIMP chronology of mylonitized Tianger granite, Xinjiang: also about the dating on hydrothermal zircon rim in granite. Acta Petrologica Sinica 22, 135–144 (in Chinese with English abstract).
Zhu, W.B., Shu, L.S., Ma, R.S., Sun, Y., 2004. Comment on "Characteristics and dynamic origin of the large-scale Jiaoluotage ductile compressional zone in the eastern Tianshan Mountains, China" by X. W. Xu, T. L. Ma, L. Q. Sun and X. P. Cai. Journal of Structural Geology 26, 2331–2335.
Zonenshain, L.P., Kuzmin, M.I., Natapov, L.M., 1990. Geology of the USSR: A Plate-Tectonic Synthesis. American Geophysical Union, Washington, D.C.(242 pp.).